TTP 10-04

January 19, 2010

Higgs Pseudo-Observables, Second Riemann Sheet and All That ‡‡

GIAMPIERO PASSARINO *

Dipartimento di Fisica Teorica, Università di Torino, Italy
INFN, Sezione di Torino, Italy

CHRISTIAN STURM †

Physics Department, Brookhaven National Laboratory,
Upton, NY 11973, USA

SANDRO UCCIRATI ‡

Institut für Theoretische Teilchenphysik, Universität Karlsruhe,
76128 Karlsruhe, Germany

The relation between physical observables measured at LHC and Tevatron and standard model Higgs pseudo-observables (production cross section and partial decay widths) is revised by extensively using the notion of the Higgs complex pole on the second Riemann sheet of the S-matrix. The extension of their definition to higher orders is considered, confronting the problems that arise when QED(QCD) corrections are included in computing realistic observables. Numerical results are presented for pseudo-observables related to the standard model Higgs boson decay and production. The relevance of the result for exclusion plots of the standard model Higgs boson for high masses (up to 600 GeV) is discussed. Furthermore, a recipe for the analytical continuation of Feynman loop integrals from real to complex internal masses and complex Mandelstam invariants is thoroughly discussed.

Keywords: Feynman diagrams, Loop calculations, Radiative corrections, Higgs physics

PACS classification: 11.15.Bt, 12.38.Bx, 13.85.Lg, 14.80.Bn, 14.80.Cp

‡‡This work is supported by the European Community's Marie Curie Research Training Network *Tools and Precision Calculations for Physics Discoveries at Colliders* under contract MRTN-CT-2006-035505, by the U.S. Department of Energy under contract No. DE-AC02-98CH10886 and by the Deutsche Forschungsgemeinschaft through Sonderforschungsbereich/Transregio 9 *Computergestützte Theoretische Teilchenphysik*.

*giampiero@to.infn.it

†sturm@bnl.gov

‡uccirati@particle.uni-karlsruhe.de

Contents

1 Introduction

The search for a mechanism explaining electroweak symmetry breaking has been a major goal for many years, in particular the search for a standard model (SM) Higgs boson, see for instance Ref. [1] and Ref. [2]. As a result of this an intense effort in the theoretical community has been made to produce the most accurate NLO and NNLO predictions, see Refs. [3–6]. There is, however, a point that has been ignored in all these calculations: the Higgs boson is an unstable particle and should be removed from the in/out bases in the Hilbert space, without destroying the unitarity of the theory. Therefore, concepts as the *production* of an unstable particle or its *partial decay widths* do not have a precise meaning and should be replaced by a conventionalized definition which respects first principles of quantum field theory (QFT).

The quest for a proper treatment of a QFT of unstable particles dates back to the sixties and to the work of Veltman [8] (for earlier attempts see Ref. [9]); more recently the question has been readdressed by Sirlin and collaborators [10]. Alternative approaches, within the framework of an effective theory can be found in Ref. [11].

In this paper we discuss the relation between physical observables and Higgs pseudo-observables by considering the extension of their definition to higher orders in perturbation theory, confronting the problems that arise when perturbative corrections in quantum electrodynamics (QED) and quantum chromodynamics (QCD) are included. Numerical results are also presented. Our work can be seen as an extension of complex-mass schemes to include complex external momenta (for previous work see also Ref. [12]), addressing systematically the question of the analytical continuation of Feynman loop integrals.

This paper is organized as follows. In Section 2 we summarize the conceptual setup. In Section 3 we present general arguments on complex poles. In Section 4 and 5 we discuss pseudo-observables, on-shell observables and unitarity. The analytical continuation of Feynman loop integrals into the second Riemann sheet of the S-matrix is examined in Section 6. In Section 7 we present the inclusion of QED and QCD corrections and renormalization schemes are highlighted in Section 8. Numerical results are given in Section 9 and in Section 10 we close with our conclusions.

2 Formulation of the problem

There are two old questions in relating measurements to theoretical predictions:

– Experimenters (should) extract so-called *realistic observables* from raw data, e.g. $\sigma(pp \to \gamma\gamma + X)$ and need to present results in a form that can be useful for comparing them with theoretical predictions, i.e. the results should be transformed into pseudo-observables; during the deconvolution procedure one should also account for the interference background – signal;

– Theorists (should) compute pseudo-observables using the best available technology and satisfying a list of demands from the self-consistency of the underlying theory [14].

Almost from the start it is clear that a common language must be established in order to avoid misunderstandings and confusion. A typical example can be found in Higgs physics where, frequently, one talks about *Higgs production cross section* or *Higgs partial decay widths*. After the discovery phase, in absence of which the future of high energy physics cannot be ascertained, one will need to probe the properties of the discovered resonance, like spin and couplings. In this case different sources will start talking about the same thing but with different languages. We will indicate a reasonable language within the context of a perturbative expansion of a gauge-invariant QFT in this paper.

The Higgs boson, as well as the W or Z bosons, are unstable particles; as such they should be removed from in/out bases in the Hilbert space, without changing the unitarity of the theory. As mentioned before, concepts as the production of an unstable particle or its partial decay widths, not having a precise meaning, are only an approximation of a more complete description. The inconsistencies associated with the on-shell LSZ formulation of an unstable external particles become particularly severe starting from two-loops, as described in Ref. [5].

Suppose that we want to combine a Higgs production mechanism, say gluon-gluon fusion, with the subsequent decay $H \to \gamma\gamma$. The process to be considered is, therefore, $pp \to \gamma\gamma + X$ and it is made of a part that defines the signal, e.g.

$$pp \to gg(\to H \to \gamma\gamma) + X, \tag{1}$$

and by a non-resonant background. The question is: how to extract from the data, without ambiguities, a pseudo-observable to be termed *Higgs partial decay width into two photons* which, at the same time, does not violate first principles? Once again, one should be aware that there is no Higgs boson in the in-state, therefore the matrix element $< \gamma\gamma\ \mathrm{out}|H\ \mathrm{in} >$ is not definable in QFT and this ill-defined quantity should be replaced by a pseudo-observable which closely resembles the intuitive concept of a decay width, can be unambiguously extracted from the data and respects all fundamental properties of the theory; in this way we replace a *non existing* observable with a conventional definition. A proposal in this direction can be found in Ref.[10]; here we revise the proposal, improving it by considering the extension to higher orders in perturbation theory, confronting the problems that arise when QED(QCD) corrections have to be included and present numerical results for Higgs physics.

At the parton level the S-matrix for the process $i \to f$ can be written as

$$S_{fi} = V_i(s)\, \Delta_{H}(s)\, V_f(s) + B_{if}(s), \tag{2}$$

where V_i is the production vertex $i \to H$ (e.g. $gg \to H$), V_f is the decay vertex $H \to f$ (e.g. $H \to \gamma\gamma$), Δ_{H} is the Dyson re-summed Higgs propagator and B_{if} is the non-resonant background (e.g. $gg \to \gamma\gamma$ boxes). In the next section we will introduce the notion of complex pole. A vertex is defined by the following decomposition [16],

$$V_f(s) = \sum_a V^a_f\,(s\,,\,\{S\})\; F^a_f\,(\{p_f\}) \tag{3}$$

where $s = -P^2_{H}$ (with $P_{H} = \sum_f p_f$), $s \oplus \{S\}$ is the set of Mandelstam invariants that characterize the process $H \to f$, V^a_f are scalar form factors and the F^a_f contain spinors, polarization vectors, etc.

3 The complex pole

In this section we introduce the notion of the complex pole [15] following closely the analysis of Ref. [17]. Let Δ_i be the lowest order propagator for particle i and $\overline{\Delta}_i$ the corresponding dressed propagator, i.e.

$$\overline{\Delta}_i = -\,\frac{\Delta_i}{1 + \Delta_i\, \Sigma_{ii}}, \tag{4}$$

Let us analyze in more details the definition of the dressed propagator: to begin with, consider a skeleton expansion of the self-energy $S = 16\,\pi^4\, i\, \Sigma$ with propagators that are resummed up to $\mathcal{O}\,(n)$ and define

$$\Delta^{(n)}_i(s) = -\,\Delta^{(0)}_i(s)\left[1 + \Delta^{(0)}_i(s)\, \Sigma^{(n)}_{ii}\left(s\,,\,\Delta^{(n-1)}_i(s)\right)\right]^{-1}, \tag{5}$$

where, omitting an overall factor $-i/(2\,\pi)^4$, the Born propagator (tensor structures are easily included) is

$$\Delta^{(0)}_i(s) = \frac{1}{s - m^2_i}. \tag{6}$$

If it exists, we define a dressed propagator as the formal limit [8]

$$\overline{\Delta}_i(s) = \lim_{n\to\infty} \Delta^{(n)}_i(s), \qquad \overline{\Delta}_i(s) = -\,\Delta^{(0)}_i(s)\left[1 + \Delta^{(0)}_i(s)\, \Sigma_{ii}\left(s\,,\,\overline{\Delta}_i(s)\right)\right]^{-1}, \tag{7}$$

which coincides with the Schwinger-Dyson solution for the propagator.

The Higgs boson complex pole (s_{H}) is the solution of the equation

$$s_{H} - M^2_{H} + \Sigma_{HH}(s_{H}) = 0, \tag{8}$$

where M_H^2 is the renormalized Higgs boson mass; here we assume that all counter-terms have been introduced to make the off-shell Green's function ultraviolet finite, respecting locality of the counter-terms. We now examine more carefully the self-energy to all orders in perturbation theory since, often, there is some confusion with statements that are formulated to all orders and applied to a truncated perturbative expansion. Now consider the, all orders, self-energy,

$$\Sigma_{HH}(s, M_H^2, \xi) = \sum_{n=1}^{\infty} \Sigma_{HH}^{(n)}(s, M_H^2, \xi)\, g^{2n}, \tag{9}$$

where ξ is the gauge parameter (extension to more than one gauge parameters is straightforward) and g is the renormalized coupling constant. From arguments based on Nielsen identities, see Ref [16], we know that

$$\frac{\partial}{\partial \xi}\, s_H = 0, \qquad \frac{\partial}{\partial \xi}\, \Sigma_{HH}(s_H, M_H^2, \xi) = 0, \tag{10}$$

i.e. the location of the complex pole is ξ independent; as a consequence the self-energy is ξ independent too, since the two differ by a renormalized quantity, obviously ξ independent. We consider first the one-loop approximation for the self-energy: from its explicit expression we are able to derive the following relation:

$$\Sigma_{HH}^{(1)}(s, M_H^2, \xi) = \Sigma_{HH\,;\,I}^{(1)}(s, M_H^2) + (s - M_H^2)\, \Phi_H(s, M_H^2, \xi). \tag{11}$$

where, in a general R_ξ gauge, we obtain

$$M_W^2\, \Phi_H = -\frac{1}{8}\Big\{(s+M_H^2)\Big[B_d(s, M_Z^2, M_Z^2; \xi_Z) + 2\, B_d(s, M_W, M_W; \xi_W)\Big] + 2\, A_d(M_Z, \xi_Z) + 4\, A_d(M_W, \xi_W)\Big\},$$

$$B_d\,(s, m, m, \xi) = B_0\,(s, \xi\, m, \xi\, m) - B_0\,(s, m, m)\,, \quad A_d\,(m, \xi) = A_0(\xi\, m) - A_0(m). \tag{12}$$

The symbols $A_0, B_0,$ etc. are the usual scalar, one-loop functions.

It needs to be stressed that the splitting between gauge dependent and gauge independent quantities is only defined modulo a ξ-independent constant. Our definition of the invariant part is that it coincides with the expression in the 't Hooft-Feynman gauge (i.e. $\xi = 1$). Furthermore, finite renormalization (i.e. replacing renormalized parameters with a set of *experimental* data points after having removed ultraviolet poles by means of local counter-terms) amounts to replace

$$M_H^2 = s_H + \Sigma_{HH}(s_H, M_H^2, \xi), \tag{13}$$

showing that

$$\frac{\partial}{\partial \xi}\, \Sigma_{HH}^{(1)}(s_H, s_H, \xi) = 0, \tag{14}$$

so that, at one-loop, the Higgs complex pole is gauge parameter independent if the self-energy is computed at $M_H^2 = s_H$, the basis of the so-called complex-mass scheme (see Ref. [18] and also Ref. [17]). From Eq.(10) and from the one-loop result in Eq.(11), we derive the following

$$\Sigma_{HH}^{(n)}(s_H, M_H^2, \xi) = \Sigma_{HH\,;\,I}^{(n)}(s_H, M_H^2) + \Sigma_{HH\,;\,\xi}^{(n)}(s_H, M_H^2, \xi),$$
$$\Sigma_{HH\,;\,\xi}^{(n)}(s_H, M_H^2, \xi) = \Sigma_{HH\,;\,I}^{(n-1)}(s_H, M_H^2)\, \Phi_H(s_H, M_H^2, \xi). \tag{15}$$

Using Eq.(15) we can rewrite Eq.(8) at the two-loop level as

$$M_H^2 = s_H + g^2\, \Sigma_{HH\,;\,I}^{(1)}(s_H, s_H) + g^4\Big[\Sigma_{HH\,;\,I}^{(2)}(s_H, s_H) + \Sigma_{HH\,;\,I}^{(1)}(s_H, s_H)\, \frac{\partial}{\partial M_H^2}\, \Sigma_{HH\,;\,I}^{(1)}(s_H, M_H^2)\Big|_{M_H^2 = s_H}\Big]. \tag{16}$$

We find as worthy note that Eq.(16) can be easily generalized to all orders in perturbation theory showing that, order-by-order, the gauge dependent part of the self-energy drops out in the equation for the complex pole of the particle. The complex pole, sitting on the second Riemann sheet of the S-matrix, is usually parametrized as

$$s_H = \mu_H^2 - i\,\mu_H\,\gamma_H. \tag{17}$$

It is worth noting that a consistent treatment of external (s) and internal (M_H^2) masses allows the extension of the complex mass scheme beyond one-loop, without the need of expanding the self-energy around $s_H = \mu_H^2$, as frequently done in the literature. In partial contrast to the traditional complex mass scheme, Ref. [18], in our approach (described in Ref. [17]) it is the finite renormalization equation and not the Lagrangian that is modified. Indeed, calling the scheme *complex mass scheme* is somehow misleading; to the requested order we replace everywhere the renormalized mass M_B^2 with $s_B + \Sigma_{BB}(s_B)$ which is real by construction; if only one-loop is needed then $M_B^2 \to s_B$ everywhere, therefore justifying the name *complex mass*.

The quest for gauge invariance and the consequent introduction of a complex pole instead of an on-shell mass signal has a certain degree of ambiguity in defining the Higgs boson mass (as well as the mass of any unstable particle). The most convenient choice, for all practical purposes, is represented by the square root of the real part of s_H, although

$$\overline{\mu}_H^2 = \mu_H\,\left(\mu_H^2 + \gamma_H^2\right)^{1/2} \tag{18}$$

also has several advantages [19] and will be used in our numerical results.

There is a final comment for this section: the complex pole for an unstable particle, parametrized according to Eq.(8), must correspond to a negative imaginary part; otherwise, even the Wick rotation cannot be safely performed. Consider the case of the Higgs boson, ii channels that do not satisfy the negativity condition for the imaginary part below the $4\,m_i^2$ (real) threshold are excluded in the evaluation of s_H. As we already mentioned the contribution to the imaginary part of s_H from a given channel below the corresponding real threshold (WW, ZZ and $\overline{t}t$) represents an approximation to the corresponding $4f$ and $6f$ cuts, i.e. $H \to WW, ZZ \to 4f$ etc, which is acceptable only when the corresponding γ_H is positive, a condition which fails at one-loop for $\overline{t}t$ intermediate states when the top quark mass is kept real; in this case $\overline{t}t$ intermediate states never contribute, in our scheme, to γ_H below threshold, i.e. they are discarded. It is interesting to note that this problem completely disappears if we allow for a top quark complex pole (instead of real on-shell mass). Numerical examples will be discussed in Section 9; unfortunately the top quark total (on-shell) width is poorly known, therefore inducing large uncertainties on the corrections. In the numerical analysis we use $\Gamma_t \leq 13.1\,\mathrm{GeV}$, based on the experimental upper limit of Ref. [20].

4 Extracting a partial decay width

In this section we examine our options to define a pseudo-observable which is related, as closely as possible, to a realistic cross section and shares as many features as possible with the corresponding on-shell definition of a partial decay width. If we insist that $|H>$ is an asymptotic state in the Hilbert space then the observable to consider will be $< f\,\mathrm{out}\,|\,H\,\mathrm{in}>$, otherwise one should realize that for stable particles the proof of the LSZ reduction formulas depends on the existence of asymptotic states

$$|\,p\,\mathrm{in}\,> = \lim_{t \to -\infty} \int d^3x\,H(x)\,i\,\overleftrightarrow{\partial}_t\,e^{i\,p\cdot x}\,|\,0\,>, \tag{19}$$

(in the weak operator sense). For unstable particles the energy is complex so that this limit either diverges or vanishes. Although a modification of the LSZ reduction formulas has been proposed long ago for unstable particles, see Ref. [21], we prefer an alternative approach where one considers extracting information on the Higgs boson directly from

$$< f\,\mathrm{out}\,|\,H\,>< H\,|\,i\,\mathrm{in}\,> + \sum_{n \neq H} < f\,\mathrm{out}\,|\,n\,>< n\,|\,i\,\mathrm{in}\,>, \tag{20}$$

for some initial state i and some final state f and where $\{n\} \oplus H$ is a complete set of states (not as in the in/out bases). As we are about to see, the price to be paid is the necessity of moving into the complex plane.

Define $\Pi_{HH}(s)$ as

$$\Pi_{HH}(s) = \frac{\Sigma_{HH}(s) - \Sigma_{HH}(s_H)}{s - s_H}, \tag{21}$$

then the, Dyson re-summed, Higgs propagator becomes

$$\Delta_{HH}(s) = (s - s_H)^{-1} \Big[1 + \Pi_{HH}(s)\Big]^{-1}, \qquad Z_H = 1 + \Pi_{HH}. \tag{22}$$

Using Eq.(22) we can write Eq.(2) as

$$S_{fi} = \Big[Z_H^{-1/2}(s)\, V_i(s)\Big] \frac{1}{s - s_H} \Big[Z_H^{-1/2}(s)\, V_f(s)\Big] + B_{if}(s). \tag{23}$$

From the S-matrix element for a physical process $i \to f$ we extract the relevant pseudo-observable,

$$S\,(H_c \to f) = Z_H^{-1/2}(s_H)\, V_f(s_H), \tag{24}$$

which is gauge parameter independent – by construction – and satisfies the relation

$$S_{fi} = \frac{S\,(i \to H_c)\; S\,(H_c \to f)}{s - s_H} + \text{non resonant terms}. \tag{25}$$

The partial decay width is further defined as

$$\mu_H\, \Gamma\,(H_c \to f) = \frac{(2\,\pi)^4}{2} \int d\Phi_f\,(P_H\,,\,\{p_f\}) \sum_{\text{spins}} \Big|S\,(H_c \to f)\Big|^2, \tag{26}$$

where the integration is over the phase space spanned by $|f>$, with the constraint $P_H = \sum p_f$. One should not confuse phase space and the real value of $s = -P_H^2$, where the realistic observable is measured, with the complex value for s, where gauge invariant loop corrections must be computed. The choice of P_H^2 (phase space) where to define the pseudo-observable is conventional, e.g. one can use the real part of s_H. Indeed, the r.h.s. of Eq.(24) satisfies the property

$$\frac{\partial}{\partial \xi}\, Z_H^{-1/2}(s_H)\, V_f(s_H) = 0 \tag{27}$$

to all orders in perturbation theory. If we define

$$V_f\,\left(s, M_H^2\right) = \sum_{n=0}^{\infty} g^{2n+1} \Big[V_{f\,;\,I}^{(n)}\left(s, M_H^2\right) + V_{f\,;\,\xi}^{(n)}\left(s, M_H^2\right)\Big], \tag{28}$$

we obtain, expanding in powers of the coupling constant g, that

$$V_{f;\,\xi}^{(1)}(s_H, s_H) = \frac{1}{2}\, V^{(0)} \Phi_H(s_H, s_H), \qquad V_{f;\,\xi}^{(2)}(s_H, s_H) = -\frac{1}{2} \Phi_H(s_H, s_H) \Big[V_{f;\,\xi}^{(1)}(s_H, s_H) - \frac{1}{4} V^{(0)} \Phi_H(s_H, s_H)\Big], \tag{29}$$

etc. One last example of a basic fact: Nielsen identities give the structure of the gauge parameter dependent vertex and self-energy order-by-order in perturbation theory. It is important to stress at this point that the renormalized mass should be replaced consistently with the use of Eq.(13).

To summarize, only s_H is a meaningful quantity and a definition of the real mass or of the total width is conventional. From Eq.(8) one has

$$\mu_H\, \gamma_H = \operatorname{Im} \Sigma_{HH}(s_H), \tag{30}$$

and it should be evident, from Eq.(26), that $\gamma_H \neq \sum_f \Gamma\,(H_c \to f)$. The reason can be understood when we consider a simple example, a toy model with $\mathcal{L}_{\text{int}} = m^2\, \phi\, \sigma^+\, \sigma^-$ (with massless σ-particles). Already at one-loop, we find

$$\operatorname{Im} \Sigma_{\phi\phi}(s) = \frac{m^2}{16\,\pi^2}\, \pi, \qquad \operatorname{Im} \Sigma_{\phi\phi}(s_\phi) = \frac{m^2}{16\,\pi^2}\, \pi \left(1 + \frac{1}{\pi} \arctan\left(\frac{\gamma_\phi}{\mu_\phi}\right)\right). \tag{31}$$

While the first relation in Eq.(31) (real s) satisfies the cutting equation [7] the second (complex s) does not. For a proper perspective it must be recalled that when we expand, $\Sigma_{HH}(s_H) = \Sigma_{HH}(\mu_H^2) + \dots$, the cutting equation is restored at NLO but it will still be violated at NNLO, as pointed out in Ref. [16]. Therefore, our conventional definition of the Higgs total decay width will be $\Gamma_{\rm tot}(H_c) = \sum_f \Gamma(H_c \to f)$.

To set the stage, it may be well to recall that the breakdown of a process into products of pseudo-observables can be generalized to include unstable particles in the final state; an example is given in Fig. 1 where the (triply-resonant) signal in $gg \to 4\,$f is split into a chain $gg \to H$ (production), $H \to W^+W^-$ (decay) and $W \to \bar{f}f$ (decays).

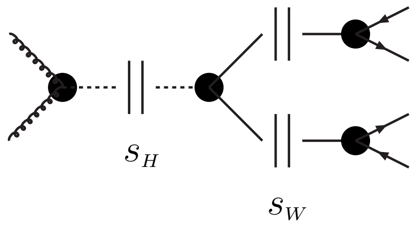

Figure 1: Gauge-invariant breakdown of the triply-resonant $gg \to 4\,$f signal into $gg \to H$ production, $H \to W^+W^-$ decay and subsequent $W \to \bar{f}f$ decays.

5 Pseudo-observables, on-shell observables and unitarity

When we consider all the possible decay channels of an *on-shell* standard model Higgs boson we obtain that up to an on-shell mass $m_H \approx 140\,$GeV the Higgs boson is very narrow while the width rapidly increases after the opening of the WW and ZZ channels.

Even this statement should be carefully examined since W and Z bosons are unstable particles to be removed from the in/out bases of the Hilbert space. For real W, Z masses the Higgs boson width is related to the cuts of the self-energy and the statement under examination is based on the (say one-loop) two-fermion cut, two-boson cut, etc.

Unitarity follows if we add all possible ways in which a diagram with given topology can be cut in two separating S from $S^\dagger$. For a stable particle the cut line, proportional to the positive energy part of the propagator, contains a pole term $2\,i\,\pi\,\theta(p_0)\,\delta(p^2+m^2)$, whereas there is no such contribution for an unstable particle. We express $\mathrm{Im}\,\Sigma$ in terms of cut self-energy diagrams and repeat the procedure ad libidum, therefore proving that cut unstable lines are left with no contribution, i.e. unstable particles contribute to the unitarity of the $S-$matrix via their stable decay products [8].

From this point of view the second cut of the Higgs self-energy (after the two-fermion cut) is the four-fermion cut, not the two-boson one (once again, the cutting of a line corresponding to an unstable particle contains no pole term). How bad is the choice of cutting two, *stable*, W boson lines with respect to cutting four fermion lines and summing over all fermions, i.e. how bad is the on-shell approach, at least from a numerical point of view?

If one evaluates the ratio

$$\Gamma\,(H \to VV)\;\mathrm{BR}\,(V \to 2f)\;\mathrm{BR}\,(V \to 2f')\;\,/\,\Gamma\,(H \to 2f + 2f') \tag{32}$$

the results of Ref. [22] show that the on-shell phase space for the WW or ZZ final state introduces an error of the order of 10% near the threshold, which is still satisfactory. Using the complex mass scheme which, in turns violates unitarity, will improve upon the on-shell result since the internal V masses are themselves complex poles. Remarkably, the complex mass scheme represents a method which is, at the same time, predictive and gives the best available approximation to the use of a full (Schwinger-Dyson) re-summed theory, a formal solution of the problem which, however, poses an insurmountable barrier for the technology of today.

6 Loop integrals with complex masses and invariants

In this section we analyze the correct definition of Feynman integrals with complex masses and Mandelstam invariants. On a more formal bases one should say that unstable states lie in a natural extension of the usual Hilbert space that corresponds to the second sheet of the S-matrix; these states have zero norm and, therefore, escape the usual prohibition of having an hermitian Hamiltonian with complex energy [21]. On a more pragmatic level we use the guiding principle that Green's functions involving unstable particles should smoothly approach the value for stable ones (the usual Feynman $-i\,0$ prescription) when the couplings of the theory tend to zero.

The whole problem can be summarized as follows: in the limit of zero couplings all particles are stable and we define Green's functions in the cut s-plane, where s is the selected invariant to be continued into the complex plane. For the *free* theory of stable particles, according to Feynman prescription, the value of the argument of some function lies, say below the cut (which coincides for example to the real negative axis); during continuation of s we may cross the cut, which means that we have to continue the function into its second branch.

For the simple case that we have just described the Green's function is then defined through its value on the principal branch in all quadrants but the second, where continuation to the second branch is required. This *new* function will have a cut on the positive imaginary axis and special problems may occur, especially when we want to do analytical continuation at the level of integrands and also internal masses in a given Feynman diagram are complex, as required by any realistic complex-mass scheme. Green's functions are given in terms of Feynman parametric integrals and our main point will be: how to define the same integrals but properly continued to complex internal masses and complex external invariants? One of the difficulties of the problem lies in having masses and invariants complex at the same time which introduces subtleties in the analytical continuation which are not present if, say only masses or only invariants are made complex.

6.1 General setup

To start our analysis, consider a scalar $\phi\,\sigma^2$ theory with $M_\phi > 2\,m_\sigma$, i.e. ϕ is unstable; the ϕ propagator (with $s = -\,p^2$) is

$$\Delta = \Big[s - M_\phi^2 + \Sigma_{\phi\phi}(s)\Big]^{-1}, \tag{33}$$

where factors $(2\,\pi)^4\,i$ have been omitted. The inverse function, $\Delta^{-1}(s)$ is analytic in the entire s-plane except for a cut from $s = 4\,m_\sigma^2$ to infinity along the real axis. The function is defined above the cut, $\Delta^{-1}(s + i\,0)$ and the analytical continuation downwards is to the second Riemann sheet, i.e.

$$\Delta_2^{-1}(s - i\,0) = \Delta^{-1}(s + i\,0) = \Delta^{-1}(s - i\,0) + 2\,i\,\pi\,\rho(s), \tag{34}$$

where $2\,i\,\pi\,\rho(s)$ is the discontinuity of the function across the cut. For a complete discussion of the analytical continuation see, e.g., Ref. [24].

We need a few definitions which will help the understanding of the procedure for the analytical continuation of functions defined through a parametric integral representation. The logarithm is defined by

$$\ln^{(k)} z = ln^{(0)} z + 2\,i\,\pi\,k, \quad k = 0\,, \pm 1\,, \pm 2\,, \dots \tag{35}$$

where $\ln^{(0)} z$ denotes the principal branch ($-\pi < \arg(z) \le +\pi$). From now on we will omit the superscript that denotes the principal branch of the logarithm. Let $z_\pm = z_0 \pm i\,0$ and $z = z_R + i\,z_I$, we define

$$\ln^{\pm}(z\,;\,z_\pm) = \Big\{ \begin{array}{l} \ln z \pm 2\,i\,\pi\,\theta\,(-z_0)\;\theta\,(\mp z_I) \\ \ln z \pm 2\,i\,\pi\,\theta\,(-z_R)\;\theta\,(\mp z_I)\,, \end{array} \tag{36}$$

i.e. the first Riemann sheet for all quadrants but the second where the function is defined in the second Riemann sheet.

Our first definition of the $\ln^{\pm}$-functions in Eq.(36) is the most natural in defining analytical continuation of Feynman integrals with a smooth limit into the theory of stable particles; the reason is simple, in case some of the particles are taken to be unstable we have to perform analytical continuation only when the corresponding Feynman diagram, in the limit of all (internal) stable particles, develops an imaginary part (e.g. above some normal threshold). However, in all cases where the analytical expression for the diagram is known, one can easily see that the result does not change when replacing z_0 with z_R, the second variant in Eq.(36).

As we are going to discuss in the following sections there are cases where one would like to perform an analytical continuation at the level of integrand in the Feynman parametric representation of a given diagram; often the integration contour has to be distorted into the complex plane with the consequence that $z_R \neq z_0$ and $\mathrm{sign}(z_R) \neq \mathrm{sign}(z_0)$. In this case we need a more general definition of $\ln^{\pm}$:

Definition: Let $z(\Gamma) \in C$ ($\Gamma \in R$) be an arbitrary complex function of Γ; when we want to continue $z_0 = z(0)$ (not in the second quadrant) to $z_f = z(\Gamma_f)$ we must look for a real Γ_c with $0 < \Gamma_c < \Gamma_f$ such that $z_c = z(\Gamma_c)$ is real and negative (for simplicity we assume the case a monotonic $z_\Gamma = z(\Gamma)$): then, $\forall \Gamma \,:\, \Gamma \geq \Gamma_c$ we replace $\ln z$ with its analytical continuation into the second Riemann sheet,

$$\ln^{\pm}(z_\Gamma\,;\, z_0) = \ln z_\Gamma \pm 2\,i\,\pi\,\theta\,(-\mathrm{Re}\, z_\Gamma)\;\theta\,(\mp \mathrm{Im}\, z_\Gamma)\,. \tag{37}$$

For all practical purposes Eq.(37) can be replaced with the second variant of Eq.(36) (with $z \to z_\Gamma$) which, from now on, will be our definition of analytical continuation.

6.2 Analytical continuation of the Euler dilogarithm

We consider now the Euler's dilogarithm, $\mathrm{Li}_2\,(z)$; if we denote its principal branch by $\mathrm{Li}_2^{(0,0)}(z)$ ($0 < \arg(z-1) < 2\,\pi$), than for any branch (see, e.g. [25]) we have

$$\mathrm{Li}_2^{(n,m)}(z) = \mathrm{Li}_2^{(0,0)}(z) + 2\,n\,\pi\,i\,\ln^{(0)} z + 4\,m\,\pi^2, \quad n\,,\,m = 0\,,\,\pm 1\,,\,\pm 2\,,\ldots \tag{38}$$

The question that we want to analyze is the following: given

$$\mathrm{Li}_2(M^2 + i\,0) = -\int_0^1 \frac{dx}{x}\,\ln\left(1 - M^2\,x - i\,0\right), \qquad \mathrm{Im}\,\mathrm{Li}_2\left(M^2 + i\,0\right) = \pi\,\ln M^2\,\theta\left(M^2 - 1\right), \tag{39}$$

how do we understand Eq.(38) in terms of an integral representation? Let us consider the analytical continuation from $z^+ = M^2 + i\,0$ to $z = M^2 - i\,M\,\Gamma$ and define

$$I = -\int_0^1 \frac{dx}{x}\,\ln^{-}\left(1 - z\,x\,;\, 1 - z^+\,x\right). \tag{40}$$

With $\chi(x) = 1 - z\,x = 1 - (M^2 - i\,M\Gamma)\,x$, we have $\chi(0) = 1$ and $\chi(1) = \left(1 - M^2\,,\, M\,\Gamma\right)$. If $M^2 > 1$ we have that χ crosses the positive imaginary axis with $\mathrm{Im}\,\chi = \Gamma/M$. As a result we obtain

$$I = \mathrm{Li}_2^{(0,0)}(z) + 2\,i\,\pi\,\ln M^2, \tag{41}$$

which is not the expected result since I does not reproduce the correct continuation of Li_2 given in Eq.(38). The mismatch can be understood by observing that $\ln^{-}$ has a cut along the positive imaginary axis (of χ) and, in the process of continuation, with $x \in [0,1]$, we have been crossing the cut. Nevertheless, we insist on defining analytical continuation at the level of integrand, instead of working directly on the result, because it is the only practical way of dealing with multi-loop diagrams where an exact result is not known. The solution consists in deforming the integration contour, therefore defining a new integral,

$$I_C = \int_C \frac{dx}{x}\,\ln^{-}\left(1 - z\,x\,;\, 1 - z^+\,x\right), \tag{42}$$

where the curve C is given by two straight segments, $0 \leq x \leq 1/M^2 - \epsilon$ and $1/M^2 + \epsilon \leq x \leq 1$ ($\epsilon \to 0^+$), plus a curve C' defined by

$$C'(u)\;:\;\{x = u + i\,\frac{1 - M^2\,u}{M\,\Gamma}\}, \quad \frac{1}{M^2 + \Gamma^2} \leq u \leq \frac{1}{M^2}, \tag{43}$$

The integral over C' is downwards on the first quadrant an upwards on the second (along the cut of $\ln^-$). Integration of $\ln^-$ over C' gives $-2\,i\,\pi\,(\ln M^2 - \ln z)$, showing that

$$\mathrm{Li}_2^{(1,0)}(z) = I_C, \tag{44}$$

the correct analytical continuation. Therefore we can extend our integral, by modifying the contour of integration, to reproduce the right analytical continuation of the dilogarithm.

6.3 Continuation of analytical results

Having introduced a simple example, we consider now one-loop two-point functions where both masses and the external invariant are made complex. Let

$$\chi(x) = s_P\,x^2 + \left(m_2^2 - m_1^2 - s_P\right)\,x + m_1^2, \tag{45}$$

$$s_P = M^2 - i\,\Gamma\,M, \qquad m_i^2 = \mu_i^2 - i\,\gamma_i\,\mu_i. \tag{46}$$

The function B_0 is originally defined, for real s_P and real (equal for simplicity) internal masses, by

$$B_0\left(M^2\,;\,\mu,\mu\right) = \frac{1}{\bar{\epsilon}} - \int_0^1 dx\,\ln(\chi - i\,0), \tag{47}$$

where $\bar{\epsilon}^{-1} = 2/(4-n) - \gamma_E - \ln\pi$ ($\gamma_E \approx 0.5772$ being the Euler-Mascheroni constant), and we need the analytical continuation to arbitrary values of s_P (i.e. $M^2 \to M^2 - i\,M\,\Gamma$ with $\Gamma > 0$); we assume, for a moment, real internal masses ($\gamma = 0$) and $M^2 > 4\,\mu^2$; the analytical result is

$$B_0\left(M^2\,;\,\mu,\mu\right) = \frac{1}{\bar{\epsilon}} - \ln\frac{\mu^2}{\mu_R^2} + 2 - \beta\,\ln\frac{\beta+1}{\beta-1}, \tag{48}$$

where μ_R is the renormalization scale and $\beta^2 = 1 - 4\,\mu^2/M^2$. For the continuation to $M^2 \to M^2 - i\,M\,\Gamma$, $\mu^2 \to \mu^2 - i\,\gamma\,\mu$ we have to compute the logarithm of $z^{\rm UST} = z_R^{\rm UST} + i\,z_I^{\rm UST}$, which is a function of Γ, γ (interacting theory of unstable particles). Let

$$z_\pm^{\rm ST} = \lim_{\Gamma,\gamma\to 0} z_R^{\rm UST} \pm i\,0 = z_R^{\rm ST} \pm i\,0, \tag{49}$$

where the $\pm i\,0$ follows from Feynman prescription $\mu^2 \to \mu^2 - i\,0$. We use the second variant of Eq.(36) and define

$$\ln^\pm\left(z^{\rm UST}\,;\,z_\pm^{\rm ST}\right) = \ln z^{\rm UST} \pm 2\,i\,\pi\,\theta\left(-z_R^{\rm UST}\right)\,\theta\left(\mp z_I^{\rm UST}\right), \tag{50}$$

which satisfies

$$\lim_{\Gamma,\gamma\to 0} \ln^\pm\left(z^{\rm UST}\,;\,z_\pm^{\rm ST}\right) = \ln z_\pm^{\rm ST}, \tag{51}$$

and it is equivalent to have $\ln z$ on the second Riemann sheet, but only when z is continued into the second quadrant. There is one awkward possibility; it corresponds to starting from $z_-^{\rm ST}$ with $z_R^{\rm ST} < 0$ and requiring continuation to $z_I^{\rm UST} > 0$ and $z_R^{\rm UST} > 0$. Using Eq.(48) we derive

$$B_0\left(M^2\,;\,m,m\right) \to \frac{1}{\bar{\epsilon}} - \ln\frac{m^2}{\mu_R^2} + 2 - \beta_c\,\ln^-\left(\frac{\beta_c+1}{\beta_c-1}\,;\,\frac{\beta+1}{\beta-1}\right) \tag{52}$$

where $\beta_c^2 = 1 - 4\,m^2/s_p$. It is worth noting that there is never a problem when internal masses are real and we continue to complex p^2. Otherwise we first continue to complex internal masses using the fact that internal (complex) squared masses have a negative imaginary part. Consider this continuation for one-loop diagrams: with L-external legs we can always fix a parametrization where the coefficient of m_1^2 is $1 - x_1$, the one of m_i^2 is $x_{i-1} - x_i$, up to m_L^2 which has coefficient x_{L-1} where the parameters satisfy $0 \le x_{L-1} \le \,\dots\, \le x_1 \le 1$ (i.e. all coefficients are non-negative). Less straightforwardly the same holds for multi-loop diagrams.

Then we continue from $\Gamma = 0$; considering Eq.(52) and denoting by ζ the ratio $(\beta_c + 1)/(\beta_c - 1)$ we have $\mathrm{Re}\,\beta_c^2 > 0$ (in the region above real thresholds) and $\mathrm{Im}\,\beta_c^2 > 0$ for $\Gamma = 0$. At $\Gamma = (M/\mu)\,\gamma$ β_c^2 crosses the positive real axis from above; this corresponds to ζ crossing the cut where we move into the second Riemann sheet of the logarithm of Eq.(52). After that one has $\mathrm{Im}\,\zeta > 0$ and the forbidden region is reached when $\mathrm{Re}\,\zeta > 0$, which corresponds to $\mid \beta_c \mid > 1$. Once again, for $\gamma = 0$ the latter is never satisfied. In general, the condition requires solving a cubic equation in Γ with only one real, negative, solution. The forbidden region requires, therefore, $\Gamma < 0$.

To continue our analysis of one-loop functions, where analytical results are known, we only need to define

$$\mathrm{Li}_2^{\mp}\left(z^{\mathrm{UST}}\,;\,z_{\mp}^{\mathrm{ST}}\right) = \mathrm{Li}_2\,(z) \mp 2\,i\,\pi\,\theta\,(z_R^{\mathrm{UST}} - 1)\;\theta\,(\pm z_I^{\mathrm{UST}})\;\ln z^{\mathrm{UST}}. \tag{53}$$

For our purposes, namely for the processes that we are considering, we only need one additional function. The most general scalar three-point function that is needed will be

$$C_0\left(0,0,p^2\,;\,m_1,m_2,m_3\right) = \frac{1}{p^2}\Big\{\sum_{i=1,3}(-1)^{\delta_{i3}}\left[\mathrm{Li}_2\left(\frac{x_0-1}{x_0-x_i}\right)-\mathrm{Li}_2\left(\frac{x_0}{x_0-x_1}\right)\right]+\ln x_0\,\eta\,(x_1-x_0\,,\,x_2-x_0)\Big\}, \tag{54}$$

with four different roots

$$x_0 = 1+\frac{m_1^2-m_2^2}{p^2}, \qquad x_3 = \frac{m_3^2}{m_3^2-m_2^2}, \qquad x_{1,2} = \frac{p^2+m_1^2-m_3^2 \mp \lambda^{1/2}\left(-p^2,m_1^2,m_3^2\right)}{2\,p^2}, \tag{55}$$

where λ is the Källen function. Analytical continuation requires the replacement $\mathrm{Li}_2 \to \mathrm{Li}_2^-$ with limiting (free theory of stable particles) cases given by

$$x_1 \to x_1 - i\,0, \qquad x_2 \to x_2 + i\,0, \qquad x_3 \to x_3 - i\,\mathrm{sign}(m_1^2-m_2^2)\,0. \tag{56}$$

As a final observation, there is no need to continue the square root β_c in Eq.(52) below threshold ($\beta_c^2 < 0$) since in this case β_c is imaginary and the change of sign when we move from the principal root is compensated in the product β_c times the logarithm.

Finally, in Eq.(54) and for one-loop processes with more scales and more than three legs one has to introduce a generalization of 't Hooft-Veltman η-functions [29] on the second Riemann sheet. The definition is as follows:

$$\ln^-(x\,y) = \ln^- x + \ln^- y + \eta^-(x,y), \tag{57}$$

$$\eta^-(x,y) = 2\,i\,\pi\Big\{\theta(x_I)\Big[\theta(-x_R)-\theta(y_I)\,\theta(-z_I)\Big]+\theta(y_I)\,\theta(-y_R)+\theta(z_I)\Big[\theta(-x_I)\,\theta(-y_I)-\theta(-z_R)\Big]\Big\}, \tag{58}$$

with $z = x\,y$ and $z = z_R + i\,z_I$ etc.

6.4 Continuation at the integrand level

We now turn to analytical continuation at the integrand level, according to our procedure where all Feynman integrals are treated according to their parametric integral representation.

Let us consider the specific example of the previous section: a scalar two-point function corresponding to two internal equal masses, $m^2 = \mu^2 - i\,\mu\,\gamma$ and $s_p = M^2 - i\,M\,\Gamma$. Due to the symmetry of $\chi(x)$, in Eq.(47) the integral with $0 \le x \le 1$ can be written as twice the same integral with $0 \le x \le 1/2$; the argument of the logarithm goes from $\mathrm{Re}\,\chi = \mu^2 > 0$ to $\mathrm{Re}\,\chi = \mu^2 - M^2/4 < 0$ (above threshold) with $\mathrm{Im}\,\chi = -\,i\,0$. We have to define the analytical continuation $M^2 \to M^2 - i\,M\,\Gamma$; since, for any x, χ cannot cross the cut, it must be analytically continued into a second Riemann sheet above the cut. A similar situation occurs for complex internal masses: the integration with respect to x is

$$\chi = \left(\mu^2\,,\,-i\,\mu\,\gamma\right) \quad \to \quad \chi = \left(\mu^2 - \frac{1}{4}\,M^2\,,\,-i\,\mu\,\gamma + \frac{i}{4}\,M\,\Gamma\right). \tag{59}$$

Let $X = x\,(1-x)$ with $0 \le X \le 1/4$, select a value for x, when $\Gamma \ge (\mu\,\gamma)(M\,X)$ continuation is into the second Riemann sheet. Of course, for $M^2 < 4\,\mu^2$, χ remains on the first Riemann sheet for all values of Γ. The variable χ is such that

$$\begin{aligned} \mathrm{Re}\,\chi = 0 \qquad &\text{for} \quad x = R_\pm = \frac{1}{2}\Big[1 \pm \sqrt{1 - 4\,\frac{\mu^2}{M^2}}\Big]. \\ \mathrm{Im}\,\chi = 0 \qquad &\text{for} \quad x = I_\pm = \frac{1}{2}\Big[1 \pm \sqrt{1 - 4\,\frac{\mu\gamma}{M\Gamma}}\Big]. \end{aligned} \tag{60}$$

The second equation requires $M\Gamma \ge 4\,\mu\gamma$ for $I_\pm$ to be real and $\in [0\,,1]$. At $x = I_\pm$ the condition $\mathrm{Re}\,\chi \le 0$ requires $\Gamma\mu \le M\gamma$. Therefore, for those values of Γ and x that satisfy the conditions

$$4\,\frac{\mu}{M}\,\gamma \le \Gamma \le \frac{M}{\mu}\,\gamma, \qquad I_- \le x \le I_+, \qquad R_- \le x \le R_+, \tag{61}$$

we have $\mathrm{Re}\chi \le 0$, $\mathrm{Im}\chi \ge 0$ and $\ln\chi$ must be continued into the second Riemann sheet.

The new definition of the B_0-function is as follows:

$$B_0 = \frac{1}{\bar{\epsilon}} - \int_0^1 dx\,\ln^-\left(\chi\,;\,\chi_-\right), \qquad \chi_- = \chi\Big|_{\Gamma,\gamma_i=0} - i\,0, \tag{62}$$

Different possibilities are illustrated in Fig. 2 where we show $\chi(x)$ for two equal (complex) internal masses.

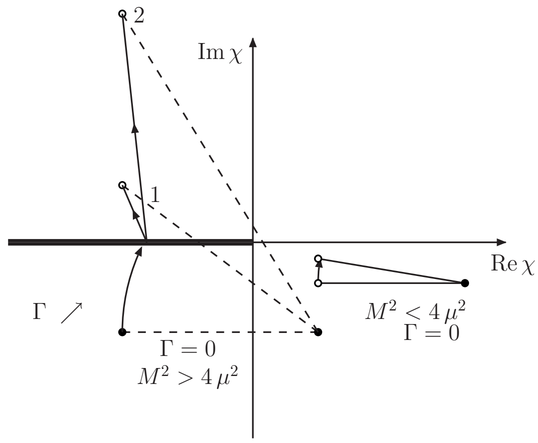

Figure 2: Analytical continuation from real p^2 to complex p^2 as seen in the χ-plane with $\chi(x) = -s_P\,x\,(1-x) + \mu^2 - i\,\mu\,\gamma$, with $s_P = M^2 - i\,M\,\Gamma$ and $x \in [0,1]$. Solid lines represent the continuation for a low value of M with a very small value for Γ. With increasing values for M we reach the situation illustrated by the dot-lines, χ moving into the second quadrant, i.e. χ on the second Riemann sheet. Case 1 holds for $\Gamma < (M/\mu)\,\gamma$ whereas case 2 holds for $\Gamma > (M/\mu)\,\gamma$. Black circles correspond to $x = 0, x = 1$ whereas white circles correspond to $x = 1/2$.

In any realistic application the complex pole equation returns, for low values of M, small values of Γ and $\mathrm{Re}\,\chi$ is always positive, never requiring analytical continuation into another sheet; when M increases Γ increases too and we find values of χ that requires the continuation $\ln \to \ln^-$. This will happen for $x \ge I_-$ in case 1 (which requires $\Gamma < (M/\mu)\,\gamma$) and for $x > R_-$ in case 2 (which requires $\Gamma > (M/\mu)\,\gamma$).

The same example can be discussed in the x complex plane; in this case, when $M > 2\,\mu$ and $\Gamma = \gamma = 0$, the cut is on the real axis between R_- and R_+ (Eq.(60)) and the integration is $0 < x < 1/2$. The integral is originally defined ($\Gamma, \gamma = 0$) above the cut, i.e. for $x + i\,0$. Analytical continuation means that for increasing imaginary parts we reach a point where the integration path is continued into the second Riemann sheet (at $\Gamma = (M/\mu)\,\gamma$, we have $I_- = R_-$ and, for higher values of Γ, the continuation to the second Riemann sheet is required as soon as the cut is reached). From this point of view the integral is better understood in terms of a variable $z(x) = u + i\,v$, such that $\chi = -M^2\,z\,(1-z) + \mu^2$ and the integration is performed along the curve

$$v\,(1-2\,u) = \frac{Z}{M^2}, \qquad Z = \mu\,\gamma - M\Gamma\,x\,(1-x), \qquad u = \frac{1-U}{2}, \qquad U^4 + \Big[4\,x(1-x) - 1\Big]\,U^2 - 4\,\frac{Z^2}{M^4} = 0. \tag{63}$$

Note that $x = I_-$ corresponds to $z = I_-$, real. For real internal masses we have $z(0) = 0$ and $z(1/2) = (\Gamma/(2M))^{1/2}\,(1 - i/2)$. In the z-plane the logarithm has a cut on the positive real axis between R_- and R_+.

It is worth mentioning that case 2 of Fig. 2 corresponds to an integration path that crosses the cut of $\ln^-$ across the positive imaginary x-axis, similar to the case of the dilogarithm discussed above. Therefore, the correct analytical continuation, for case 2, goes as follows: the integration path in z-space (Eq.(63)) is moved into the complex plane and goes into the lower half-plane instead of reaching the cut of the logarithm (which is between R_- and R_+, see also Fig. 3).

In order to insure that the analytically continued integral has a smooth limit $\Gamma, \gamma \to 0$ we deform the integration path by insisting that the cut (of ln) must be crossed at $z = R_-$ (note that for case 2 we have $I_- < R_-$) where we perform a continuation into the second Riemann sheet. In this way we add to B_0 (on top of a factor $-\,2\,i\,\pi\,\beta$) a new contribution which is easily computed in the x-plane and it is related to the discontinuity of $\ln\chi$ along a curve C parametrized by

$$C(t)\;:\;\{x = \frac{1-t}{2} + i\,f(t)\}, \qquad f(t) = \frac{1}{2}\Big\{-\,\frac{\Gamma}{M}\,t + \Big[\Big(1 + \frac{\Gamma^2}{M^2}\Big)\,t^2 - \beta^2\Big]^{1/2}\Big\}, \tag{64}$$

with $\beta^2 = 1 - 4\,\mu^2/M^2 > 0$ and where $\bar{\beta} < t < \beta$; here $\bar{\beta}$ is the value of t where $\mathrm{Re}\,\chi(t) = \mathrm{Im}\chi(t) = 0$. The integral over C is on the segment $\mathrm{Re}\,\chi = \pm\epsilon$ with $\epsilon \to 0^+$, from $\mu^2\Gamma/M - \mu\gamma > \mathrm{Im}\chi > 0$ on the first Riemann sheet and from $\mu^2\Gamma/M - \mu\gamma < \mathrm{Im}\chi < 0$ on the second Riemann sheet. Therefore, we have to add to B_0 an additional term $-\,2\,i\,\pi\,\Delta\,A$ with

$$\Delta A = A(\bar{\beta}) - A(\beta), \qquad A(t) = \Big(1 + i\,\frac{\Gamma}{M}\Big)\,t - i\,\Big[\Big(1 + \frac{\Gamma^2}{M^2}\Big)\,t^2 - \beta^2\Big]^{1/2}. \tag{65}$$

Note that in the limit $\Gamma, \gamma \to 0$ we have $\bar{\beta} \to \beta$ and this additional term vanishes. Furthermore, $A(\beta) = \beta$ and $A(\bar{\beta}) = \beta_c$, with $\beta_c^2 = 1 - 4\,m^2/s_p$. Therefore, we reproduce the correct result of Eq.(52). The recipe is, therefore, replace ln with $\ln^-$ in the integrand but deform the integration contour in order to avoid crossing of the positive imaginary χ-axis when this would occur.

In summary, our result with a simple example we observe that

$$\mathrm{Li}_n \overset{\text{Analyt.Cont.}}{\longmapsto} \mathrm{Li}_n^-, \quad \mathrm{Li}_{n+1}^-(z) \neq \int_0^z \frac{dx}{x}\,\mathrm{Li}_n^-(x), \tag{66}$$

since deformation of the integration contour is required for the general case.

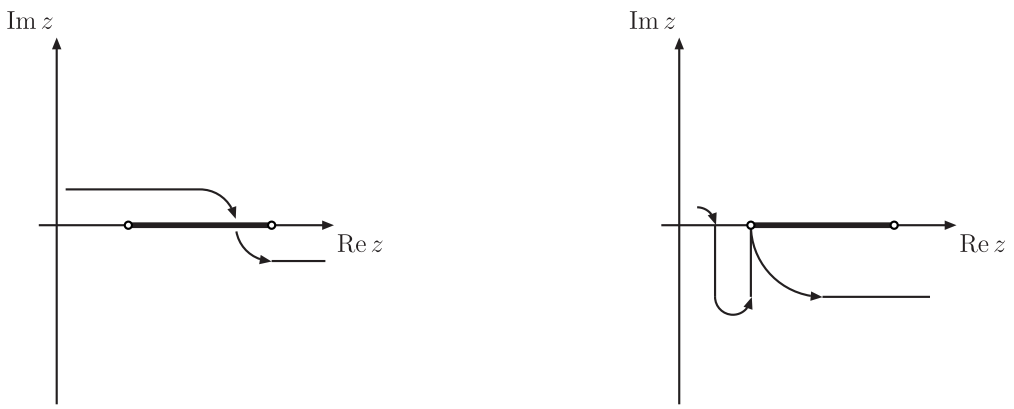

Figure 3: Analytical continuation of a B_0-function as seen in the z-plane with a cut along the positive real axis between R_- and R_+ (Eq.(60)). In the first part the integration path reaches the point I_- (Eq.(60)) and continuation after $z = I_-$ is in the second Riemann sheet. In the second part, where $I_- < R_-$ continuation must be, once again, in the second Riemann sheet; therefore the integration path which has moved into the lower half-plane must be deformed to cross the cut before moving once more into the lower half-plane (but on the second Riemann sheet).

6.5 Narrow width approximation

The practical implementation for higher point (or higher loop) functions presents a formidable technical problem, due to the higher dimension of the x-space; more will be explained in Section 6.6 but, for this reason, we have also considered analytical continuation in narrow-width-approximation (hereafter NWA). Here we replace ln with $\ln^-$ (or $\ln^+$) at the integrand level and do not perform any deformation of the integration (hyper-)contour. The resulting expression is expect to have a range of validity given by $\Gamma \ll M$. Numerical investigation of the Higgs complex pole shows that NWA returns reliable results when compared with the exact expression. The rationale for analytical continuation in NWA is based on the fact that, as we are going to show, all higher-point (higher-loop) functions admit integral representations with integrand of logarithmic nature (one-loop) or, at most, of poly-logarithmic nature (multi-loop).

Consider now the extension to complex variables of an arbitrary scalar three-point function C_0 (in NWA), defined by

$$C_0 = \int_0^1 dx_1 \int_0^{x_1} dx_2 \, V^{-1-\epsilon/2}(x_1, x_2), \tag{67}$$

where $n = 4 - \epsilon$ and V is a quadratic form

$$V(x_1, x_2) = a\, x_1^2 + b\, x_2^2 + c\, x_1\, x_2 + d\, x_1 + e\, x_2 + f - i\,0 \equiv x^t\, H\, x + 2\, K^t\, x + L, \tag{68}$$

whose coefficients are related to the internal masses and the external momenta by the relations $H_{ij} = -\, p_i \cdot p_j$, $L = m_1^2$ and

$$K_1 = \frac{1}{2}\,(p_1 \cdot p_1 + m_2^2 - m_1^2), \quad K_2 = \frac{1}{2}\,(P \cdot P - p_1 \cdot p_1 + m_3^2 - m_2^2), \tag{69}$$

with $P = p_1 + p_2$. Let us define the usual Bernstein - Sato - Tkachov (hereafter BST) factors (see Ref. [27]) as $B_3 = L - K^t\, H^{-1}\, K$ and BST co-factors $X = -\, H^{-1}\, K$. It is convenient to introduce special notations, $X_0 = 1$, $X_3 = 0$, and $V(\widehat{i\, i+1})$ to denote contractions, i.e.

$$V(\widehat{0\,1}) = V(1, x_1), \quad V(\widehat{1\,2}) = V(x_1, x_1), \quad V(\widehat{2\,3}) = V(x_1, 0). \tag{70}$$

In this way we obtain a simple integral representation

$$C_0 = \frac{1}{B_3} \Big\{ \frac{1}{2} + \int_0^1 dx_1 \, \Big[\int_0^{x_1} dx_2 \, \ln V(x_1, x_2) - \frac{1}{2} \sum_{i=0}^{2} (X_i - X_{i+1}) \ln V(\widehat{i\, i+1}). \Big] \Big\}. \tag{71}$$

When some or all the invariants are complex, $P^2 = -\, s_P$ with $s_P = M^2 - i\,\Gamma\, M$ and $m_i^2 = \mu_i^2 - i\,\gamma_i\,\mu_i$ (in realistic cases, e.g. decay of an unstable particle, $p_{1,2}^2$ are real) we define

$$V_- = V\Big|_{\Gamma, \gamma_i = 0}, \tag{72}$$

which includes the $-\,i\,0$ prescription and write

$$\begin{aligned} C_0 = \frac{1}{B_3} \Big\{ \frac{1}{2} &+ \int_0^1 dx_1 \, \Big[\int_0^{x_1} dx_2 \, \ln^- \left(V(x_1, x_2)\, ;\, V_-(x_1, x_2) \right) \\ &- \frac{1}{2} \sum_{i=0}^{2} (X_i - X_{i+1}) \, \ln^- \Big(V(\widehat{i\, i+1})\, ;\, V_-(\widehat{i\, i+1}) \Big) \Big] \Big\}. \end{aligned} \tag{73}$$

For instance, with $P^2 = -M^2 + i\, M\, \Gamma$, $p_{1,2}^2 = 0$ and $m_{1,3} = 0$, $m_2^2 = \mu^2 - i\,\mu\,\gamma$ we find that when $\Gamma/\gamma \leq \mu/M$ $\ln V$ must be continued to the second Riemann sheet for $0 \leq x_2 \leq (\mu\gamma)/(M\Gamma)$.

Starting with an integral representation of a three-point function where the integrand is the logarithm of a polynomial in parametric space is the safest way of performing analytical continuation; of course, going beyond NWA requires contour deformation but even the latter admits a consistent numerical implementation.

Nor should one fail to notice 't Hooft and Veltman emphasis, in their seminal work [29], on this subject: they put up warning signs about continuation of their result to complex momenta.

For higher point functions ($L = D, E, F, \dots$) we apply the BST algorithm [30] as many times as it is needed to produce logarithms in the integrand and proceed by replacing ln with $\ln^-$,

$$L = \int_{\{x\}} d\{x\} \,\ln\left(\chi(\{x\}) - i\,0\right) \to \int_{\{x\}_{C(\chi)}} d\{x\} \,\ln^- \,\chi(\{x\}), \tag{74}$$

where $\{x\}$ is the $x_1, \dots, x_n$ simplex and $\{x\}_{C(\chi)}$ is the path that avoids crossing the positive imaginary χ-axis. NWA amounts to the identification $\{x\}_{C(\chi)} \equiv \{x\}$.

For multi-loop integrals other functions must be extended, e.g. we will use Eq.(53), with similar results for all generalized Nielsen polylogarithms [26]

$$S^-_{n,p}(z^{\rm UST};z^{\rm ST}_-) = S_{n,p}(z^{\rm UST}) + \sum_{k=1}^{p} \frac{(-2i\pi)^k}{k\,!}\left[S_{n,p-k}(z^{\rm UST}) - \sum_{j=0}^{n-1}\frac{\ln^j z^{\rm UST}}{j\,!}S_{n-j,p-k}(z^{\rm UST})\right]\theta(z^{\rm UST}_R - 1)\,\theta(z^{\rm UST}_I), \tag{75}$$

which is derived by using $\ln^+$ in the integral representation of the generalized Nielsen polylogarithms. Since it has been shown that multi-loop diagrams can be written as integrals of multivariate generalized Nielsen polylogarithms [31] our recipe gives the analytical continuation to all orders in perturbation theory, but one does have to be careful in one respect: using familiar relations such as splitting of logarithms should be done with a grain of salt.

6.6 Analytical continuation and contour deformation

Exact analytical continuation at the integrand level can be performed by deforming the integration contour into the complex parametric space (for a general treatment see Ref. [28]). In this case we need the general definition of $\ln^-$ given in Eq.(37).

To illustrate contour deformation we consider, once again, the case of a B_0-function with equal (complex) internal masses. If

$$M > 2\,\mu \qquad \mu\,\Gamma - M\,\gamma > 0, \tag{76}$$

the function $\chi(x), x \in [0, \frac{1}{2}]$ crosses the positive imaginary axis (the branch cut of $\ln^-$). To avoid crossing we deform the x-integration into

$$\begin{aligned} &1) \qquad x = i\,\frac{\Gamma}{M}\,\beta\,t, \\ &2) \qquad x = \frac{1}{2}\,t + i\,\frac{\Gamma}{M}\,\beta\,(1-t), \end{aligned} \tag{77}$$

with $t \in [0, 1]$ and β a free parameter. For $\chi^{(1)}$ we require ${\rm Im}\,\chi^{(1)}(t) < 0, \forall t \in [0, 1]$; this is possible if $\beta < \beta_{\rm max}$, with

$$\beta_{\rm max} = \frac{1}{2}\,\frac{M^2}{\Gamma^2}\,\left[1 + \sqrt{1 + 4\,\frac{\mu\,\gamma\,\Gamma}{M^3}}\right]. \tag{78}$$

For $\chi^{(2)}$ we require that ${\rm Re}\,\chi^{(2)}(t) = 0$ corresponds to ${\rm Im}\,\chi^{(2)}(t) < 0$, which requires $\beta > \beta_{\rm min}$, where $\beta_{\rm min}$ is the largest, real, solution of the following equation

$$\mu\,\left(\frac{\Gamma}{M^2} - \frac{1}{4\,\Gamma}\right)\,(\Gamma\,\mu - M\,\gamma)\,(\beta^2 - 1) + \left[\frac{1}{4}\,\left(M^2 + \Gamma^2\right) - \mu\,\left(\mu + \frac{\Gamma\,\gamma}{M}\right)\,\right]\beta = 0. \tag{79}$$

For $\beta_{\rm min} < \beta < \beta_{\rm max}$ we have that $\chi^{(1,2)}$ never cross the positive imaginary axis. Furthermore, we compare $\chi^{(1,2)}(0)$ with $\chi^{(1,2)}(\Gamma)$ at fixed $t \in [0, 1]$ and replace $\ln \to \ln^-$ when (always at fixed t) $\chi^{(1,2)}(\Gamma)$ crosses the negative real axis for some value Γ_c. In the example that we are considering, illustrated in Fig. 4, everything is particularly simple since ${\rm Im}\,\chi({\rm Re}\,\chi)$ is always a straight line but our recipe works, as well, in the general case and allows for a straightforward algorithmic implementation.

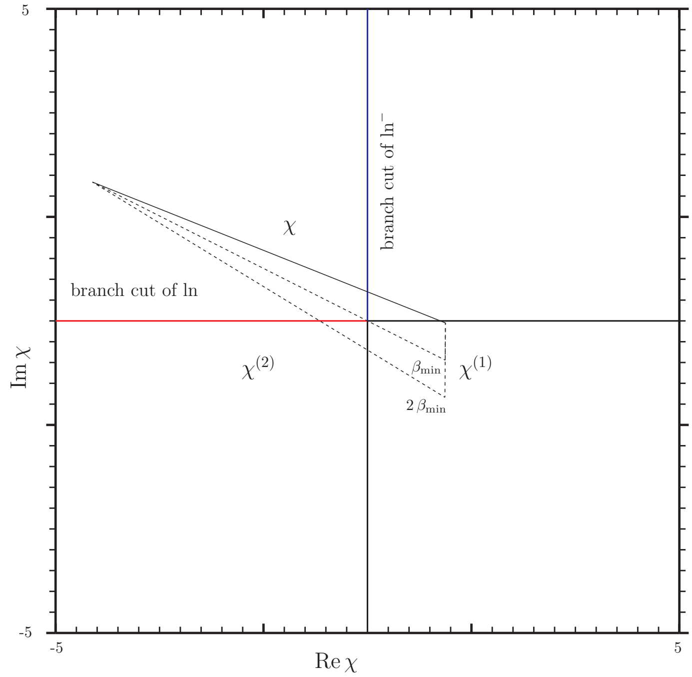

Figure 4: Example of contour deformations in computing a scalar two-point functions with equal (complex) internal masses and complex p^2.

For a general recipe of contour deformation, we proceed by analyzing the case where a Feynman diagram can be written as:

$$\int_0^1 dx_1 \cdots dx_n \sum_i A_i(x_1, \ldots, x_n)\, \ln V_i(x_1, \ldots, x_n), \tag{80}$$

where V_i are multivariate polynomials in $x_1, \ldots, x_n$, at most quadratic in each variable (note that all one-loop diagrams can be written according to Eq.(80), see Ref. [27]); actually the procedure works as well when each V_i is a quadratic form in, at least, one variable. For each term in the sum, we select one variable $x \equiv x_i$ (among $x_1, \ldots, x_n$) and study the analytical continuation (assuming that $\mathrm{Im}[V]_{\text{real masses}} < 0$)

$$\ln V \to \ln^- V \qquad \text{with} \qquad V = a\,x^2 + b\,x + c, \tag{81}$$

where a, b, c are polynomials in the remaining Feynman variables. The idea is to deform only the x integration contour into the complex plane (when needed) while keeping all other variables $(x_1, \ldots, x_{i-1}, x_{i+1}, \ldots, x_n)$ on the real axis. We define

$$a = a_r + i\,a_i \qquad b = b_r + i\,b_i \qquad c = c_r + i\,c_i \qquad x = u + i\,v. \tag{82}$$

The real and imaginary parts of V are then given by:

$$\begin{aligned}
\mathrm{Re}V &= a_r\,u^2 - 2, a_i\,u\,v - a_r\,v^2 + b_r\,u - b_i\,v + c_r \\
&= a_r\,(u-u_c)^2 - 2\,a_i\,(u-u_c)\,(v-v_c) - a_r\,(v-v_c)^2 + \delta_r, \\
\mathrm{Im}V &= a_i\,u^2 + 2, a_r\,u\,v - a_i\,v^2 + b_i\,u + b_r\,v + c_i \\
&= a_i\,(u-u_c)^2 + 2\,a_r\,(u-u_c)\,(v-v_c) - a_i\,(v-v_c)^2 + \delta_i,
\end{aligned} \tag{83}$$

where we introduced the following auxiliary variables:

$$x_c = u_c + i\,v_c = -\frac{a^*\,b}{2\,|a|^2}, \qquad \delta = \delta_r + i\,\delta_i = c - \frac{a^*\,b^2}{4\,|a|^2}. \tag{84}$$

The curves Re$V = 0$ and Im$V = 0$ are hyperbolas with center in x_c. We also define an auxiliary function,

$$U = -a_i \, \mathrm{Re}V + a_r \, \mathrm{Im}V = 2\,|a|^2\,(u - u_c)\,(v - v_c) + a_r\,\delta_i - a_i\,\delta_r. \tag{85}$$

The curve $U = 0$ is again an hyperbola with center in x_c and asymptotes parallel to the u and v axes. The branch-cut of $\ln^- V$ in the x complex plane is defined by:

$$\text{cut}: \qquad \mathrm{Re}V = 0 \;\&\; \mathrm{Im}V \geq 0 \qquad \Longleftrightarrow \qquad \begin{cases} \mathrm{Re}V = 0 \;\&\; U \geq 0, & \text{if } a_r > 0, \\ \mathrm{Re}V = 0 \;\&\; U \leq 0, & \text{if } a_r < 0. \end{cases} \tag{86}$$

First we study the intersection of the curve Re$V = 0$ with the real u axis. If $\Delta = b_r^2 - 4\,a_r\,c_r < 0$, the hyperbola Re$V = 0$ never crosses the real axis and there is no need of contour deformation (this is the first case of Fig. 5). If $\Delta \geq 0$, the intersections are given by:

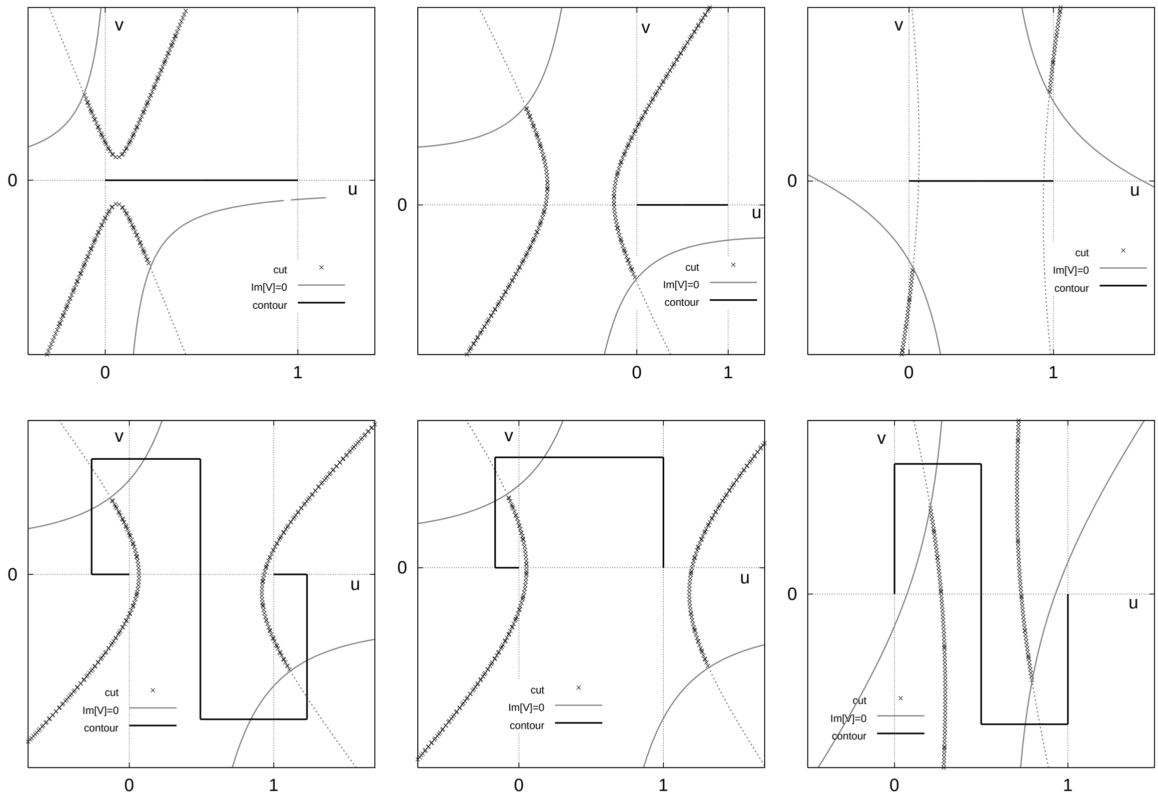

Figure 5: Examples of deformation in the x-complex plane ($x = u + iv$) of the integration contour $[0, 1]$ for integral of $\ln^- V = \ln^-(ax^2 + bx + c)$.

$$\mathrm{Re}V = 0 \;\&\; v = 0 \qquad \Longrightarrow \qquad u = u_0^{\pm} = \frac{-b_r \pm \sqrt{\Delta}}{2\,a_r}. \tag{87}$$

If both solutions are not in $[0, 1]$ a distortion is not needed (second plot in Fig. 5). Even if $u_0^{\pm} \in [0, 1]$, it can happen that the intersection occurs for Im$V < 0$ (as in the third case of Fig. 5) and there is no need of deformation to avoid the cut. In order to understand whether it occurs, we can study where the zeros of V (Re$V =$ Im$V = 0$) are lying. This system of equations has always two and only two solutions $x_\pm = u_\pm + i\,v_\pm$, whose real and imaginary parts are given by:

$$u_\pm = u_c \pm \sqrt{|\sigma| + \sigma_r}, \qquad v_\pm = v_c \pm \mathrm{sign}\,(\sigma_i)\,\sqrt{|\sigma| - \sigma_r}, \qquad \sigma = -\frac{a^*\,\delta}{2\,|a|^2}. \tag{88}$$

Note that these points are also solution of the equation $U = 0$ and (because of the simple form of U) we can conclude that:

$$
\text{cut}:\ \ \mathrm{Re}V = 0\ \&\ \mathrm{Im}V \geq 0\ \ \Leftrightarrow\ \begin{cases} \mathrm{Re}V = 0\ \&\ U \geq 0\ \ \Leftrightarrow\ \ \mathrm{Re}V = 0\ \&\begin{cases} v \geq v_+ & \text{if}\ \ u > u_c \\ v \leq v_- & \text{if}\ \ u < u_c \end{cases} & \text{if}\ a_r > 0, \\ \mathrm{Re}V = 0\ \&\ U \leq 0\ \ \Leftrightarrow\ \ \mathrm{Re}V = 0\ \&\begin{cases} v \leq v_+ & \text{if}\ \ u > u_c \\ v \geq v_- & \text{if}\ \ u < u_c \end{cases} & \text{if}\ a_r < 0. \end{cases} \tag{89}
$$

At this point we have all information to fix the new integration contour, starting from $x = 0$ and ending at $x = 1$ without crossing the branch-cut. Of course, as long as the cut is not crossed, all integration contours are equivalent and give the same result: it may fairly be said that we have some freedom in defining the deformation and that, at the same time, we can control the correctness of the result by using different paths. The general situation is depicted in the fourth plot of Fig. 5 and the new integration contour is defined by seven segments:

$$
\begin{array}{ll}
(1) & x\ =\ -\alpha_1\, t, \\
(2) & x\ =\ -\alpha_1 + i\,\beta_1\, t, \\
(3) & x\ =\ -\alpha_1\,(1-t) + \alpha_c\, t + i\,\beta_1, \\
(4) & x\ =\ \alpha_c + i\,\beta_1\,(1-t) + \beta_2\, t, \\
(5) & x\ =\ \alpha_c\,(1-t) + (1+\alpha_2)\, t + i\,\beta_2, \\
(6) & x\ =\ 1 + \alpha_2 + i\,\beta_2\,(1-t), \\
(7) & x\ =\ (1+\alpha_2)\,(1-t) + t.
\end{array} \tag{90}
$$

The coefficients α_1, β_1, α_2, β_1 and α_c can be fixed according to the principle of the minimal deformation to avoid crossing the cut. This gives the following conditions:

$$
\begin{array}{lllll}
\alpha_1 > \ \ |u_-| & \text{if} & 0 \leq u_0^- \leq 1 & \& \quad u_- \leq 0, & \alpha_1 = 0 \quad \text{otherwise}, \\
\begin{cases} \beta_1 > \ \ |v_-| \\ \beta_1 < -\,|v_-| \end{cases} & \text{if} & 0 \leq u_0^- \leq 1 & \& \quad \begin{array}{l} v_- \geq 0\ \&\ a_r > 0, \\ v_- \leq 0\ \&\ a_r < 0, \end{array} & \beta_1 = 0 \quad \text{otherwise}, \\
\alpha_2 > \ \ |u_+| & \text{if} & 0 \leq u_0^+ \leq 1 & \& \quad u_+ \geq 1, & \alpha_2 = 0 \quad \text{otherwise}, \\
\begin{cases} \beta_2 < -\,|v_+| \\ \beta_2 > \ \ |v_+| \end{cases} & \text{if} & 0 \leq u_0^+ \leq 1 & \& \quad \begin{array}{l} v_+ \leq 0\ \&\ a_r > 0, \\ v_+ \geq 0\ \&\ a_r < 0, \end{array} & \beta_2 = 0 \quad \text{otherwise}, \\
\begin{cases} \alpha_c = \ \ u_c \\ \alpha_c = \ \ 0 \\ \alpha_c = \ \ 1 \end{cases} & \text{if} & \begin{array}{l} 0 \leq u_0^- \leq u_0^+ \leq 1, \\ u_0^- \leq 0 \leq u_0^+ \leq 1, \\ 0 \leq u_0^- \leq 1 \leq u_0^+, \end{array} & & \alpha_c = 0 \quad \text{otherwise}.
\end{array} \tag{91}
$$

The case where all coefficients vanish corresponds to non-deformation: in this case the paths in Eq.(90) are

$$
(1),\, (2),\, (3),\, (4)\ \ x = 0, \quad (5)\ \ x = t, \quad (6),\, (7)\ \ x = 1, \tag{92}
$$

and refer to $0 \leq x \leq 1$ on the real axis. Note that the case $\Delta < 0$ (where $u_0^{\pm}$ are not defined) belongs to this class. This general recipe for contour deformation works also in special cases where not all segments are needed. For example, in the fifth plot of Fig. 5 the new contour consists of only four segments: using in Eq.(90) the conditions of Eq.(91) ($\alpha_2 = \beta_2 = 0, \alpha_c = 1$), the last three segments reduce in this case to the point $x = 1$.

We can now consider in this framework the example of a B_0 function with two equal masses. In this case we have:

$$
V(x) = -s_P\, x\,(1-x) + m^2 = (-M^2 + i\, M\,\Gamma)\, x\,(1-x) + \mu^2 - i\,\mu\,\gamma, \tag{93}
$$

which corresponds to

$$
x_c = \frac{1}{2}, \qquad \delta = c - \frac{a}{4} = \mu^2 - \frac{M^2}{2} - i\,\Big[\mu\,\gamma + \frac{M\,\Gamma}{2}\Big],
$$

$$\sigma = \frac{1}{8} - \frac{a^* c}{2|a|^2} = \frac{1}{8} - \frac{\mu}{2M}\,\frac{\mu M + \gamma\Gamma}{M^2+\Gamma^2} + i\,\frac{\mu}{2M}\,\frac{\mu\Gamma - M\gamma}{M^2+\Gamma^2}. \tag{94}$$

Since $a_r > 0$, the cut crosses the segment $[0,1]$ when $\sigma_i \le 0$ (implying that $v_- \ge 0$, $v_+ \le 0$), a situation which occurs for $\mu\Gamma - M\gamma \ge 0$. It can be verified by explicit calculation that, in this case, we always have $0 \le u_\pm \le 1$, which corresponds to the situation depicted in the last diagram of Fig. 5 and the deformation requires five segments ($\alpha_1 = \alpha_2 = 0$, i.e. the first and the last segment in Eq.(90) reduce to a point).

6.7 Differential operators in a complex domain

The procedure of analytical continuation at the basis of Eq.(80) deserves an additional comment: how can we apply a differential operator at the integrand level, in order to get Eq.(80)? As an example we consider the integral of Eq.(67) on which we want to apply the BST algorithm:

$$C_0 = \int_0^1 dx \int_0^x dy\, \chi^{-1+\epsilon/2}(x,y), \qquad \epsilon \to 0^+, \tag{95}$$

where χ is a quadratic form. As we know Eq.(80) follows from BST functional relation; in order to apply the BST algorithm in the complex domain ($\chi \in C[x,y]$) we introduce

$$\Big[\chi\Big]_\pm^\mu = \exp\left(\mu\, \ln^\pm \chi\right), \tag{96}$$

and distort the integration path so that it never crosses the positive imaginary axis of χ^- (or the negative imaginary axis of χ^+). The $(-)$ analytical continuation of C_0 is defined by

$$C_0^- = \int_{\Lambda=0} dxdy\, \Big[\chi(x,y)\Big]_-^{-1+\epsilon/2}, \tag{97}$$

where $\Lambda(x,y) = 0$ is the implicit equation for the integration contour. In practice we change variables, $x = \alpha_i\, t + \beta_i$ ($t \in [0,1]$) with $i = 1,\dots,n$, n being the number of segments needed to avoid crossing the cut (e.g. see Eq.(90)). The BST functional relation [27] for quadratic forms and the corresponding linear differential operator are

$$\chi^\mu\left([x]\right) = \mathcal{D}\left(\mu\,,\,[x]\,,\,[\partial_x]\right)\, \chi^{\mu+1}\left([x]\right), \qquad \mathcal{D} = \frac{1}{B}\Big[1 - \frac{1}{2\,(\mu+1)}\sum_{i=1}^n \left(x_i - X_i\right)\partial_{x_i}\Big], \tag{98}$$

where $[x] = x_1\,,\dots,x_n$. Consider the following integral,

$$F_- = \int_{z_i\ \Gamma}^{z_f} dz\, \Big[\chi(z)\Big]_-^\mu\,, \tag{99}$$

where Γ is a curve connecting z_i and z_f which never crosses the positive imaginary axis of χ for $z \in \Gamma$. Let z_f be in the second quadrant and z_i outside of it; let z_0 be the point where $\mathrm{Im}\,\chi(z_0) = 0$, $\mathrm{Re}\,\chi(z_0) < 0$.

Thanks to the $-$ prescription the integrand in Eq.(99) is a continuous function of z (for $z \in \Gamma$) and we can write

$$F_- = F_-^{(1)} + F_-^{(2)} = \int_{z_i\ \Gamma}^{z_0} dz\, \Big[\chi(z)\Big]_-^\mu + \int_{z_0\ \Gamma}^{z_f} dz\, \Big[\chi(z)\Big]_-^\mu. \tag{100}$$

In the first integral $\big[\chi\big]_-^\mu = \chi^\mu$ and we can apply the BST relation of Eq.(98). In the second one we find

$$\begin{aligned} F_-^{(2)} &= \int_{z_0\ \Gamma}^{z_f} dz\, \Big[\chi(z)\Big]_-^\mu = \int_{z_0\ \Gamma}^{z_f} dz\, \exp\{-\,2\,i\,\pi\,(\mu+1)\}\, \chi^\mu(z) \\ &= \int_{z_0\ \Gamma}^{z_f} dz\, \exp\{-\,2\,i\,\pi\,(\mu+1)\}\, \mathcal{D}\left(\mu,z,\partial_z\right)\, \chi^{\mu+1}(z) = \int_{z_0\ \Gamma}^{z_f} dz\, \mathcal{D}\left(\mu,z,\partial_z\right)\, \Big[\chi(z)\Big]_-^{\mu+1}, \end{aligned} \tag{101}$$

where we have used $\exp\{-2i\pi\mu\} = \exp\{-2i\pi(\mu+1)\}$, showing extension of the BST algorithm into the second sheet. Note that the BST relation in the second equality of Eq.(101) is of pure algebraic nature and that the integration over Γ will always be parametrized in terms of a $\Gamma(t) \,:\, t \in R$ so that $\chi \in C[t]$ and $\mathcal{D} \in C[t] < \partial_t >$.

Each segment of Eq.(90) is of the type considered in $F_-^{(1)}$, $F_-^{(2)}$ or F_- and therefore we can apply the BST algorithm to C_0^-. It goes without saying that this is the correct procedure, instead of applying BST first and performing analytical continuation only in a second step. The result reads as follows:

$$C_0^- = \sum_{i=1}^{n} \alpha_i \, \frac{J_i}{B_3}, \qquad J_i = \int_0^1 dx \int_0^{\alpha_i x+\beta_i} dy \, \ln^-\chi(\alpha_i x+\beta_i, y) - \frac{1}{2} \sum_{j=1}^{4} \int_0^{a_{ij}} dx \, A_{ij} \, \ln^- \chi_{ij} + \frac{\alpha_i}{2} + \beta_i, \qquad (102)$$

$$\chi_{i1} = \chi(\alpha_i+\beta_i, x), \qquad \chi_{i2} = \chi(\beta_i, x), \qquad \chi_{i3} = \chi(\alpha_i x+\beta_i, \alpha_i x+\beta_i), \qquad \chi_{i4} = \chi(\alpha_i x+\beta_i, 0), \qquad (103)$$

$$A_{i1} = \frac{\alpha_i+\beta_i-X}{\alpha_i}, \quad A_{i2} = -\,\frac{\beta_i-X}{\alpha_i}, \quad A_{i3} = X-Y, \quad A_{i4} = Y, \quad a_{i1} = \alpha_i+\beta_i, \quad a_{i2} = \beta_i, \quad a_{i3} = a_{i4} = 1, \qquad (104)$$

where B_3 is the BST factor and X, Y are the BST co-factors.

With this example we have shown how to apply differential operators when complex momenta are present: first the analytical continuation has to be performed together with the deformation of the integration contour and just at the end the differential operator can be correctly applied.

In conclusion we have shown a practical implementation of the concept that the pole at the mass of a stable particle can move into other Riemann sheets where it describes an unstable particle. It is worth noting that all cases encountered so far, where both the internal masses and the Mandelstam invariants are complex, have never been discussed in the literature, although this step represents the logical extension of the complex-mass scheme, allowing for a meaningful introduction of pseudo-observables.

7 Including QED(QCD) corrections

In this section we will consider the inclusion of QED(QCD) corrections, both virtual and real. The choice $s = s_H$ in Eq.(24) is dictated by the request of a gauge independent definition of pseudo-observables and follows, once again, from Nielsen identities. Consider a final state where the inclusion of real QED(QCD) corrections is mandatory in order to obtain an infrared finite quantity, e. g. $i \to H \to \overline{b}b$. Here, at one-loop, we have wave-function renormalization factors for the external fermions and vertex corrections; the QED part generates, in the so-called $(\epsilon\,,\, m_b)$ regulator scheme (dimensional regularization for the infrared and masses for the collinear limit), a simple infrared pole and double as well as simple collinear logarithm. According to our recipe the QED(QCD) vertex correction should be evaluated at complex Higgs momentum squared. Let us define

$$s_H = x_H\,\mu_H^2, \quad \beta_c^2 = 1 - 4\,\frac{m_b^2}{s_H}, \quad \beta^2 = 1 - 4\,\frac{m_b^2}{\mu_H^2}. \qquad (105)$$

The residue of the infrared (virtual) pole reads as follows

$$R_{\rm virt} = {\rm Re}\,\frac{\beta}{\beta_c}\,\Big[\frac{\beta^2}{x_H} + 2 - \frac{1}{x_H}\Big]\,\ln^-\frac{\beta_c - 1}{\beta_c + 1}. \qquad (106)$$

The infrared pole from real emission originates from the end-point singularity in the phase space integration, where $P_H = p_b + p_{\overline{b}}$ and P_H^2 is arbitrary but real, unless one is willing to extend the phase space definition into the complex plane where δ functions are defined in terms of contour integrals [23]. Using the most obvious choice, namely $P_H^2 = -\mu_H^2$ we obtain for the (real) infrared residue

$$R_{\rm real} = \big(\beta^2 + 1\big)\,\ln\frac{1-\beta}{1+\beta}. \qquad (107)$$

Therefore, as expected, cancellation of infrared divergences is spoiled by the need of defining virtual corrections at a complex value of s. However, the fact that $Z_{_H}^{-1/2}(s)\,V_f(s)$ is gauge parameter independent only at the complex pole does not exclude a gauge independent sub-set of corrections that can be evaluated at arbitrary s. Consider the situation at the one-loop level; here, in front of the $\mathcal{O}(\alpha)$ QED corrections we use $Z_{_H} = 1$ and the one-loop vertex, $V^{\rm QED}_{\overline{b}b}$, is gauge independent for all values of s. If we introduce

$$Z_{_H} = 1 + \frac{g^2}{16\,\pi^2}\,\delta Z_{_H}, \tag{108}$$

for the wave-function renormalization factor, we can use

$$S\left(H_c \to \overline{b}b\right) = -\,\frac{g}{2}\,\frac{m_b}{M_{_W}}\,\Big\{1 + \frac{g^2}{16\,\pi^2}\,\Big[V^{\rm EW}_{\overline{b}b}(s_{_H}) - \frac{1}{2}\,\delta Z_{_H}(s_{_H})\Big] + \frac{\alpha}{4\,\pi}\,V^{\rm QED}_{\overline{b}b}(\mu^2_{_H})\Big\}, \tag{109}$$

thus preserving gauge invariance without spoiling infrared safety. Following a well established convention it is also convenient to define a *deconvoluted* pseudo-observable where QED(QCD) corrections are subtracted according to theory.

There is an intriguing alternative for the treatment of QED(QCD) corrections; since the definition of the Higgs boson mass is not unique, we could keep it as a free parameter, $M_{_H}$. Then, cancellation of infrared poles at the one-loop level requires

$$s_{_H} = x_{_H}\,M^2_{_H}, \quad \beta^2_c = 1 - 4\,\frac{m^2_b}{s_{_H}}, \quad \beta^2 = 1 - 4\,\frac{m^2_b}{M^2_{_H}}, \tag{110}$$

and $R_{\rm virt} = R_{\rm real}$. Therefore, there is a value of $M_{_H}$ which is infrared safe,

$$M^2_{_H} = |s_{_H}|\,\Big\{1 + 2\,\frac{m^2_b}{|s_{_H}|}\,\Big[1 - \mu_{_H}\,\left(\mu^2_{_H} + \gamma^2_{_H}\right)^{-1/2}\Big] + \mathcal{O}\left(m^4_b\right)\Big\}. \tag{111}$$

Figure 6: Examples of mixed electroweak-QED two-loop diagrams contributing to $H \to \overline{b}b$. The solid lines, attached to the Higgs boson (dash-line) represent Z/ϕ^0 or W/ϕ fields.

The main question in establishing the consistency of the procedure, definition of QED(QCD) corrections and their subsequent deconvolution, is about the extendability to higher orders. Using the following expansions

$$Z_{_H} = 1 + \sum_{n=1}^{\infty}\frac{g^{2n}}{16\,\pi^2}\,\delta Z^{(n)}_{_H}, \quad V_{\overline{b}b} = \sum_{n=1}^{\infty}\frac{g^{2n-1}}{16\,\pi^2}\,V^{(n-1)}_{\overline{b}b}, \quad V^{(0)}_{\overline{b}b} = -\,\frac{m_b}{2\,M_{_W}} \tag{112}$$

and working at $\mathcal{O}\left(g^5\right)$ we will have terms like

$$\delta Z^{(1)}_{_H}\,V^{(1)\,;\,\rm QED}_{\overline{b}b}, \tag{113}$$

which are of the mixed type, electroweak-QED, and where $Z_{_H}$ cannot be evaluated at arbitrary values of s. In Eq.(113) $V^{(1)\,;\,\rm QED}_{\overline{b}b}$ is the one-loop QED triangle contributing to $H \to \overline{b}b$.

However, we also have mixed two-loop diagrams, as given in Fig. 6. There is a well-known identity which allows us to extract the infrared behavior of these two-loop diagram, in terms of the product of two one-loop

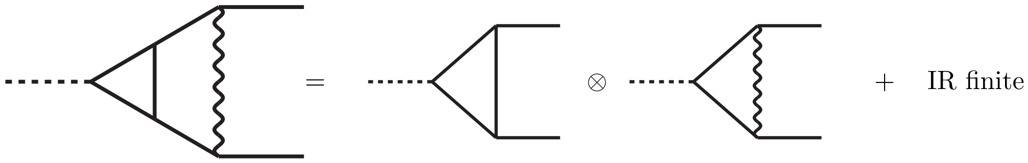

Figure 7: Infrared decomposition of a mixed electroweak-QED two-loop diagram. Here the scalar case is presented, i.e. the spin structure has been completely neglected and, for instance, the wavy line represents a scalar massless line.

vertices plus an infrared finite reminder (see [32] for the explicit decomposition in the scalar case). The decomposition for the scalar case is illustrated in Fig. 7 where the external lines in both one-loop vertices are on-shell. By scalar we mean those contributions that do not have powers of the integration momentum in the numerator.

As we have seen, the identity holds at the amplitude level, reflecting the factorization of virtual infrared corrections and the fact that virtual infrared poles are always coming from C_0-functions (the scalar ones). These identities follow from the fact that any diagram with an infrared photon line of momentum $q_i + K$, where K is a certain combination of external momenta as well as of the other loop momenta, gives an infrared divergence equivalent to the same diagram evaluated at $q_i = -K$. We thus see that the infrared decomposition into products of tensor integrals times infrared C_0-functions follows trivially. The explicit form of infrared factorization, at the amplitude level, is illustrated in Fig. 8 which shows a class of diagrams contributing to the two-loop amplitude for $H \to \overline{b}b$.

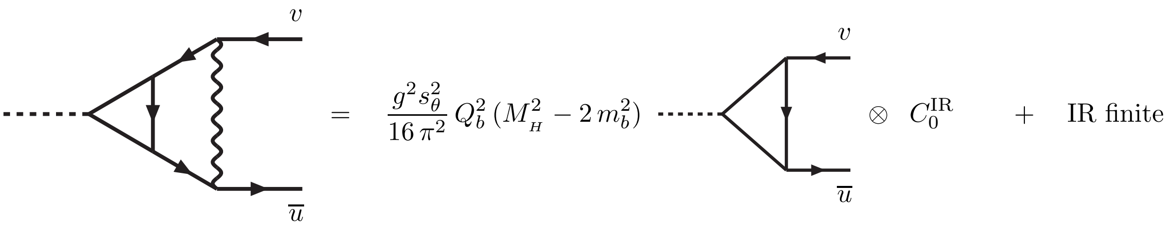

Figure 8: Infrared decomposition of a mixed electroweak-QED two-loop amplitude. Solid lines represent Z, ϕ^0 or W, ϕ particles; Dirac spinors for the external lines are included and C_0^{IR} is the scalar, infrared divergent, three-point function.

When added to the contribution coming from $\delta Z_H^{(1)}\, V_{\overline{b}b}^{(1)}$, the combination

$$V_{\overline{b}b}^{(1)\mathrm{EW}}(s) - \frac{1}{2}\,\delta Z_H^{(1)}(s) \tag{114}$$

arises naturally in front of an infrared C_0. Therefore, our recipe will be to evaluate Eq.(114) at $s = s_H$ while keeping the remaining QED-like C_0 functions (the infrared divergent ones) at $s = \mu_H^2$. The difference with the original diagram is non resonant and mixes with infrared divergent background contributions, e.g. from boxes.

For one-loop real emission we have diagrams as illustrated in the l.h.s. of Fig. 9 where we use $p_H^2 = -s_H$ and where the infrared singularity arises from the end-point of phase space integration which is controlled by a real Higgs boson momentum. The corresponding amplitude is gauge independent by construction, a fact that can be easily seen in the infrared divergent soft approximation, the r.h.s. of Fig. 9, where we have introduced the eikonal factor

$$J_{\mathrm{eik}}(p) = -\,Q_b\,\frac{p\cdot\epsilon}{p\cdot k}, \qquad \epsilon(k)\cdot k = 0, \tag{115}$$

ϵ being the photon polarization. The vertex correction, first diagram in the r.h.s. of Fig. 9, when summed with $Z_H^{-1/2} \otimes$ LO gives a gauge invariant contribution if both are evaluated at the Higgs complex pole.

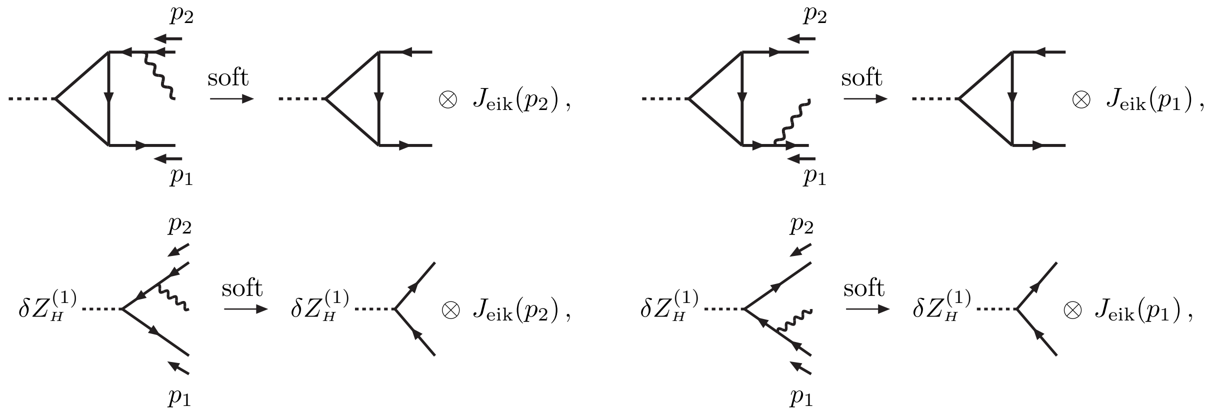

Figure 9: Examples of the infrared decomposition of $\mathcal{O}\left(g^3\right)$ electroweak diagrams with real photon emission. The last term in the r.h.s of the equation is the corresponding eikonal factor of Eq.(115).

There is another example where the introduction of QED corrections seems to be controversial if only internal masses are made complex[1]. Let us consider the pseudo-observable $\Gamma\,(H \to W^+W^-)$, with on-shell external vector bosons and internal complex masses: the infrared behavior of the one-loop corrections is reducible to a scalar vertex

$$C_0\left(-M^2_{_W}\,,\,-M^2_{_W}\,,\,-s\,,\,s_{_W}\,,0\,,s_{_W}\right), \tag{116}$$

where the difference $s_{_W} - M^2_{_W}$ ($s_{_W}$ being the W complex pole) acts as an infrared regulator, removing the infrared virtual pole,

$$C_0\left(-M^2_{_W}\,,\,-M^2_{_W}\,,\,-s\,,\,s_{_W}\,,0\,,s_{_W}\right) = \frac{2}{\beta_{_W}\,s}\,\ln\frac{\beta_{_W}+1}{\beta_{_W}-1}\,\ln\frac{s_{_W}-M^2_{_W}}{s} + \dots \tag{117}$$

where $\beta^2_{_W} = 1 - 4\,M^2_{_W}/s$. If we continue the external masses the result is instead

$$C_0\left(-s_{_W}\,,\,-s_{_W}\,,\,-s\,,\,s_{_W}\,,0\,,s_{_W}\right) = \frac{1}{\beta_{c{_W}}\,s}\,\ln^-\frac{\beta_{c{_W}}+1}{\beta_{c{_W}}-1}\,\frac{1}{\bar{\epsilon}} + \text{IR finite}, \tag{118}$$

where $\beta^2_{c{_W}} = 1 - 4\,s_{_W}/s$. Let us consider a realistic example, e.g. $gg \to 4\,$f of Fig. 1; for the complete process there is no problem at all because a photon attached to an internal W boson line cannot be infrared divergent. However, the goal is a breakdown of the full process into three components, one of which is the pseudo-observable $\Gamma\,(H \to W^+W^-)$; in order to define $\Gamma\,(H \to W^+W^-(\gamma))$ it is important to control the cancellation between virtual and real infrared corrections and, in this case, the extension to external complex masses is more than an option.

8 Schemes

For processes which are relevant for the LHC and, in particular, for $H \to \overline{b}b$, $\gamma\gamma$, gg and $gg \to H$ etc, we define three different schemes and compare their results. The schemes are:

- the RMRP scheme which is the usual on-shell scheme where all masses and all Mandelstam invariants are real;
- the CMRP scheme [5], the complex mass scheme with complex internal W and Z poles (extendable to top complex pole) but with real, external, on-shell Higgs, W, Z , etc. legs and with the standard LSZ wave-function renormalization;

[1]This point was raised by Thomas Binoth in one of our last conversations.

- the CMCP scheme, the (complete) complex mass scheme with complex, external, Higgs (W, Z, etc.) where the LSZ procedure is carried out at the Higgs complex pole (on the second Riemann sheet).

The introduction of three different schemes does not reflect a theoretical uncertainty; only the CMCP scheme is fully consistent and comparisons only serve the purpose of quantifying deviations of more familiar schemes from the CMCP scheme.

9 Numerical results

In this section we examine the numerical impact of computing Higgs pseudo-observables at the Higgs complex pole (on the second Riemann sheet of the S-matrix). We use the parametrization $s_H = \mu_H^2 - i\,\mu_H\,\gamma_H$ for the Higgs complex pole where now μ_H is an input parameter and γ_H is computed in the standard model. In this case μ_H plays the role of an input parameter while we prefer $\overline{\mu}_H^2$ of Eq.(18) as conventional definition of the Higgs boson *mass*. The results are compared with on-shell pseudo observables.

As input parameters for the numerical evaluation we have used the following values

$$M_W = 80.398\,\text{GeV}, \qquad M_Z = 91.1876\,\text{GeV}, \qquad m_t = 170.9\,\text{GeV}, \qquad \Gamma_W = 2.093\,\text{GeV},$$

$$G_F = 1.16637\,\times\,10^{-5}\,\text{GeV}^{-2}, \qquad \alpha(0) = 1/137.0359911, \qquad \alpha_S\,(M_Z) = 0.118, \qquad \Gamma_Z = 2.4952\,\text{GeV}.$$

For the W, Z complex poles we use

$$s_V = \mu_V^2 - i\,\mu_V\,\gamma_V, \quad \mu_V^2 = M_V^2 - \Gamma_V^2, \quad \mu_V\gamma_V = \,M_V\,\Gamma_V\,\left(1 - \frac{1}{2}\,\frac{\Gamma_V^2}{M_V^2}\right). \tag{119}$$

In computing $H \to gg(gg \to H)$ we have used a running $\alpha_S(\mu_H)$ (CMRP) or $\alpha_S(\overline{\mu}_H)$ (CMCP). Results for the computed γ_H are collected in Tab. 1.

μ_H [GeV]	100	120	160	170	180	200	250	400
γ_H [GeV]	0.051	0.043	0.105	0.391	0.637	1.448	4.296	39.729
γ_H [GeV]	0.051	0.043	0.105	0.391	0.637	1.448	4.373	39.829
γ_H [GeV]	0.051	0.043	0.105	0.391	0.637	1.498	5.069	40.847

Table 1: Standard model prediction for γ_H in GeV as a function of μ_H. The first entry corresponds to a real on-shell top quark mass, the second entry to a top quark complex pole derived from $\Gamma_t = \Gamma_t^{\rm NLO} = 1.31$ GeV and the last entry to a top quark complex pole derived from Γ_t equal to the experimental upper bound of 13.1 GeV.

For the evaluation of all one-loop functions in the CMCP scheme where, sometimes, a continuation to the second Riemann sheet is required we used both the analytical results and the exact numerical integration; the two in-house (independent) libraries return results in excellent agreement (typically on the sixth digit on one-loop percentage radiative corrections).

9.1 Numerical differences between the CMRP and CMCP schemes

For a better understanding of comparisons we define weak corrections to $H \to \overline{b}b$ as

$$\Delta_{\rm weak} = \sqrt{2}\,\frac{G_F\,\overline{\mu}_H^2}{\pi^2}\,\left(C_{\rm part} + B_{\rm part} + R\right), \qquad \overline{\mu}_H^2 = \mu_H\,\left(\mu_H^2 + \gamma_H^2\right)^{1/2}, \tag{120}$$

separating the corrections into a part coming from three-point functions($C_{\rm part}$), two-point functions($B_{\rm part}$) and a rational term(R). It is worth noting that there are, in general, strong cancellations among the three contributions: for instance, at 120 GeV we have a $C_{\rm part}$ of $-8.233\,\%$ from CMCP exact while the bracket in Eq.(120) is $-0.790\,\%$.

Differences between the two schemes are roughly of $\mathcal{O}\left(\gamma_{H}/\mu_{H}\right)$, as expected, and become significant above the $\overline{t}t$-threshold where the Higgs boson width becomes larger and larger. Since the width of an heavy Higgs boson is large it is natural to investigate the goodness of the separation of the production stage from the decay process. In general these stages are not independent and may be interconnected by radiative effects. Our results confirm the theorem of Ref. [33]: radiative effects are not enhanced in totally inclusive pseudo-observables with respect to the naive $\mathcal{O}\left(\gamma_{H}/\mu_{H}\right)$ argument, unless the Higgs boson is very heavy, in which case this ratio is large (at $\mu_{H} = 500\,$GeV it reaches 29%) and typical cancellations in the total weak correction factor are disturbed, increasing the effect.

To further understand the differences between the two schemes for high values of μ_{H}, we recall the well-known fact that the Higgs wave-function renormalization shows an inverse β-behavior at the W, Z threshold. In the two schemes, exactly at threshold, we will have

$$\beta^2 = 1 - 4\,\frac{\mu_B^2 - i\,\gamma_B\,\mu_B}{m_H^2}\Big|_{\rm thr} = i\,\frac{\gamma_B}{\mu_B}, \qquad \beta_c^2 = 1 - 4\,\frac{\mu_B^2 - i\,\gamma_B\,\mu_B}{\mu_H^2 - i\,\gamma_H\,\mu_H}\Big|_{\rm thr} \sim i\,\frac{\mid 2\,\gamma_B - \gamma_H \mid}{2\,\mu_B}, \tag{121}$$

where $B = W, Z$. The parameter that regularizes the divergence is therefore $\gamma_B - \gamma_H/2$ with some sizable effect around the ZZ threshold. To analyze differences between the CMRP and CMCP schemes we fix μ_H and compute γ_H; then we use Eq.(120) and compare results with the limit $\gamma_H = 0$. Results are given in Tab. 2 where we see variations induced by a finite γ_H.

γ_H/μ_H	$C_{\rm part}$	$B_{\rm part}$	R	tot
0	-3.673	-1.999	$+4.514$	-1.658
0.03	-3.760	-1.990	$+4.009$	-1.741
0	-0.308	-0.130	$+3.450$	$+3.058$
0.29	-0.986	$+0.974$	$+2.714$	$+2.702$

Table 2: Variations (in percent) at $\mu_H = 300, 500\,$GeV in the components of the total weak corrections to $H \to \bar{b}b$ according to Eq.(120).

9.2 Testing the NWA approximation

In order to analyze the quality of the NWA approximation (Section 6.5) we have considered the pure one-loop weak corrections to the decay width $H \to \overline{b}b$. It turns out, that up to $\mu_H = 250\,$GeV (where $\gamma_H/\mu_H = 0.011$) the approximation is very good, less than 1% (of a $\approx$ 1% correction). Note that analytical continuation of three-point functions in the exact CMCP scheme is required above 220 GeV.

9.3 Complete set of results

As far as the Higgs boson production cross section in gluon-gluon fusion is concerned we find that the effect of replacing the on-shell scheme (for the external Higgs boson) with the complex-pole one is completely negligible (around $3-4$ per mill) for low values of the Higgs mass, a fact that is largely expected. Only for higher values, say starting from the $\overline{t}t$ threshold, where γ_H becomes larger and larger, we reach sizable differences, above 10% and rapidly increasing.

- $\mathbf{H \to \gamma\gamma, gg, \;\; gg \to H}$

A detailed comparison of predictions in the CMRP and CMCP schemes for $H \to \gamma\gamma, gg$ is shown in Fig. 10. The partial decay width $H \to gg$ is shown in Fig. 11 where we compare the CMRP(=RMRP) and CMCP

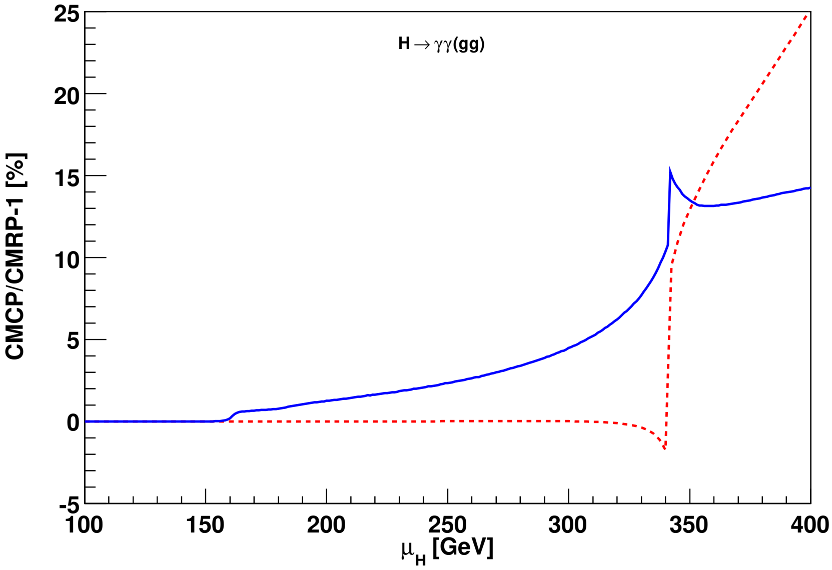

Figure 10: Comparison of predictions in the CMRP and CMCP schemes for the decays $H \to \gamma\gamma$ (blue, solid line) and for $H \to gg$ (red, dashed line). See Section 8 for the scheme definitions.

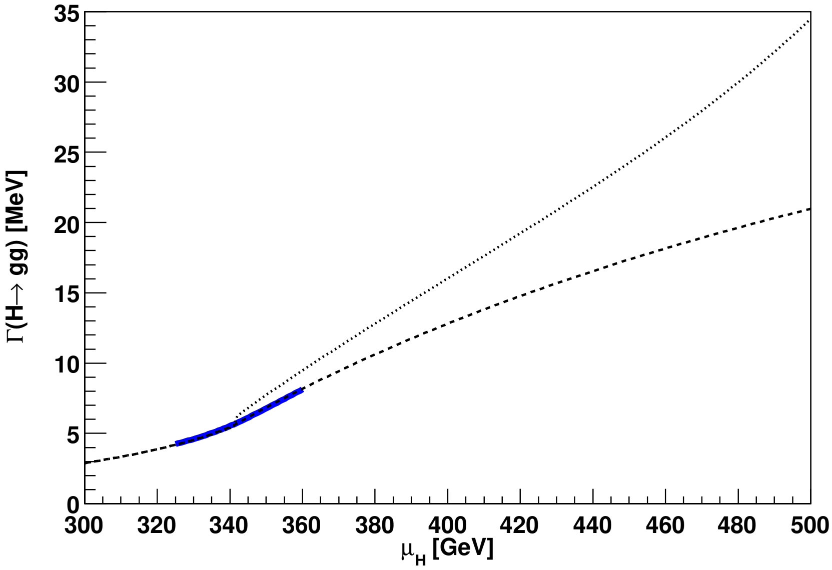

Figure 11: Comparison of the decay width $\Gamma(H \to gg)$ in the CMRP (dashed line) and the CMCP (dotted line) scheme in the high mass region. The effect of a complex top quark pole in CMCP (with a top total, on-shell, width of 13.1 GeV) is given by the blue, solid line. See Section 8 for the scheme definitions.

schemes. Similarly we compare the partial decay width $H \to \gamma\gamma$ in the RMRP, CMRP and CMCP schemes in Fig. 12.

The relatively large effects in $\Gamma(H \to \gamma\gamma)$ or $\Gamma(H \to gg)$ at large values of μ_H are still compatible with the naive $\mathcal{O}(\gamma_H/\mu_H)$ argument. Consider Fig. 10 for $\Gamma(H \to \gamma\gamma)$; for instance, at $\mu_H = 365\,$GeV we have $\gamma_H/\mu_H = 0.065$ with a variation between the CMRP and CMCP schemes of 13.3% giving a correction

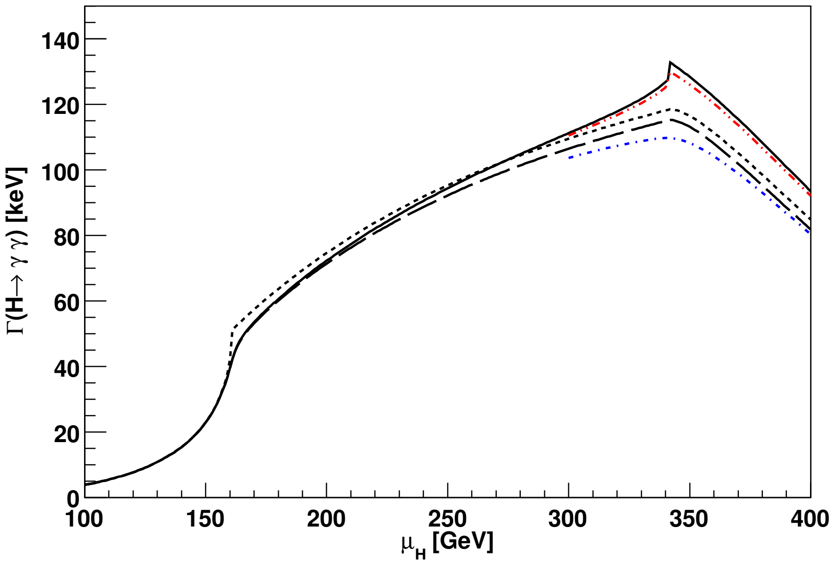

Figure 12: Comparison of the decay width $\Gamma(H \to \gamma\gamma)$ in the RMRP (dotted line), the CMRP (dashed line) and the CMCP (solid line) scheme. The effect of a complex top quark pole in CMCP (with a top total, on-shell, width of 13.1 GeV) is given by the blue, dash-dotted line. The red, dash-double-dotted line corresponds to a top width of 1.31 GeV. See Section 8 for the scheme definitions.

factor of $2\,\gamma_H/\mu_H$. Clearly, the large increase in the Higgs boson width for increasing values of μ_H makes it questionable to use a perturbative description for the Higgs-resonant part of $pp \to X$ when we have a very heavy Higgs boson.

The relevance of this result is clear: if a light Higgs boson is not discovered, one of the goals of LHC will be to exclude a standard model Higgs up to 600 GeV [37]; already at 500 GeV we have

$$\frac{\sigma_{\rm CMCP}(gg \to H)}{\sigma_{\rm CMRP}(gg \to H)} = 1.64, \qquad \text{parton level}, \tag{122}$$

comparable to the effect of NLO QCD corrections. We have computed also $\sigma(pp \to H)$ in the two schemes using MSTW 2008 LO parton distribution functions (PDF) [34]. The ratio is given in Fig. 13, for different values of s; in this figure we present

$$\frac{\sigma_{\rm CMCP}(pp \to H)}{\sigma_{\rm CMRP}(pp \to H)}, \tag{123}$$

where the numerator is evaluated at $\overline{\mu}_H$ (Eq.(18)) while the denominator corresponds to μ_H. Here we use

$$\sigma(pp \to H) = \sigma_0\,\tau_H\,\frac{dL^{gg}}{d\tau_H}, \qquad \frac{dL^{gg}}{d\tau} = \int_\tau^1 \frac{dx}{x}\,g\,(x,\mu_F)\;g\left(\frac{\tau}{x},\mu_F\right), \tag{124}$$

where $\tau = \mu_H^2(\overline{\mu}_H^2)/s$, σ_0 is the parton level cross section and g is the gluon PDF (with factorization scale $\mu_F = \mu_H$ for CMRP and $\mu_F = \overline{\mu}_H$ for CMCP).

Note that this ratio is only an indicator of the (large) size of the effect since, for a realistic value of the cross section, NLO(NNLO) QCD corrections should be included, see Ref. [35] for updated cross sections at the Tevatron and the LHC.

In Fig. 14 we show the corresponding cross section for $\sqrt{s} = 3\,$TeV, including an estimate of the uncertainty induced by varying renormalization and factorization scales (kept equal for simplicity); $\mu_H/2 \le \mu_R = \mu_F \le 2\,\mu_H$ for CMRP and $\overline{\mu}_H/2 \le \mu_R = \mu_F \le 2\,\overline{\mu}_H$ for CMCP ($\overline{\mu}_H$ is given in Eq.(18)). In Fig. 14 we do not include the uncertainty associated to PDFs.

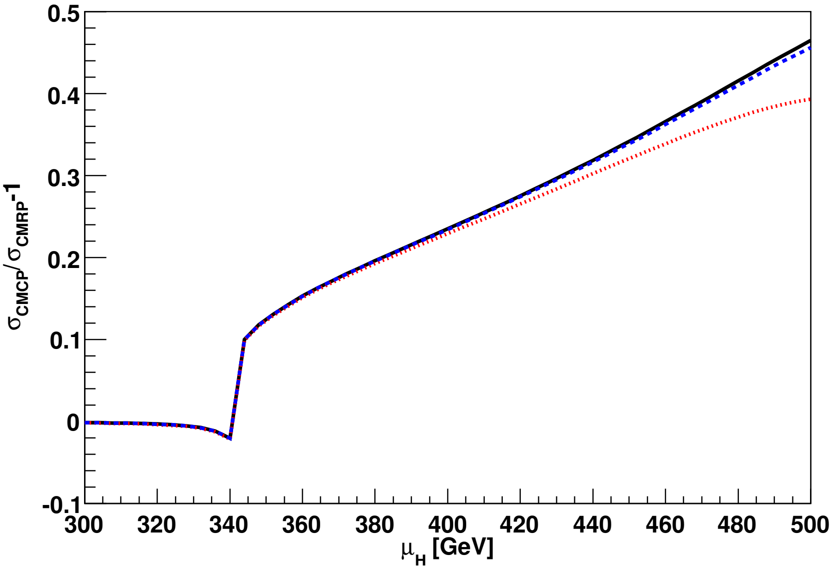

Figure 13: The ratio $\sigma_{\rm CMCP}/\sigma_{\rm CMRP}$ for the production cross section $pp \to H$, as a function of μ_H, for different energies, $\sqrt{s} = 3\,$TeV (red, dotted line), $\sqrt{s} = 10\,$TeV (blue, dashed line) and $\sqrt{s} = 14\,$TeV (black, solid line). The cross sections are computed with MSTW2008 LO PDFs with factorization scale $\mu_F = \mu_H$ for CMRP and $\mu_F = \overline{\mu}_H$ for CMCP.

The ratio between the two cross sections is stable under these variations, e.g. is between 1.4546 and 1.4574 at $\sqrt{s} = 10\,$TeV and $\mu_H = 500\,$GeV. The production cross sections for $\sqrt{s} = 10, 14$ TeV are shown in Fig. 15; note that here we use $\alpha_S(M_Z) = 0.13934$ to be consistent with the LO PDFs [34].

In order to better understand the numerical differences in the three schemes we show in Fig. 16 a scalar two-point function with two internal Z masses. In the RMRP scheme both the internal masses and the Mandelstam invariant μ_H^2 are real; in the CMRP scheme we replace M_Z^2 with the corresponding complex pole, s_Z; finally, in the CMCP scheme, also the invariant becomes complex and equal to s_H. In Fig. 16 we vary μ_H between 100 GeV and 500 GeV where $\gamma_H = 146.89\,$GeV is huge; here deviations between CMRP and CMCP become sizable. This simple example shows the general features of one-loop corrections in the three schemes; CMRP - CMCP smoothly interpolate the RMRP results around normal thresholds and, when μ_H^2 becomes larger and larger, CMCP starts deviating from RMRP - CMRP.

We also consider the expression for the amplitude $A\,(H \to \gamma\gamma)$ which can be split into a part containing only C_0-functions and a rational term. We write

$$\Gamma\,(H \to \gamma\gamma) = \frac{\alpha^2\, G_F}{32\,\sqrt{2}\,\pi^3}\,\frac{\mid s_W \mid^2}{\overline{\mu}_H}\,\Big|A\Big|^2. \tag{125}$$

If we introduce auxiliary variables,

$$\overline{\mu}_H^2 = \mu_H\,\left(\mu_H^2 + \gamma_H^2\right)^{1/2}, \quad x_t = \frac{m_t^2}{\overline{\mu}_H^2}, \quad x_H = \frac{s_H}{\overline{\mu}_H^2}, \quad x_W = \frac{s_W}{\overline{\mu}_H^2}, \tag{126}$$

the amplitude can be written as $A = A_C + R$ where

$$\begin{aligned} A_C &= -\frac{8}{3}\,x_t\,\frac{x_H - 4\,x_t}{x_W}\,C_0\,(0\,,\,0\,,\,-s_H\,,\,m_t\,,\,m_t\,,\,m_t) + 6\,\left(x_H - 2\,x_W\right)\,C_0\,(0\,,\,0\,,\,-s_H\,,\,s_W\,,\,s_W\,,\,s_W)\,, \\ R &= -\frac{16}{3}\,\frac{x_t}{x_W} + \frac{x_H}{x_W} + 6. \end{aligned} \tag{127}$$

A comparison for the real and imaginary parts in the CMRP and CMCP schemes is shown in Fig. 17.

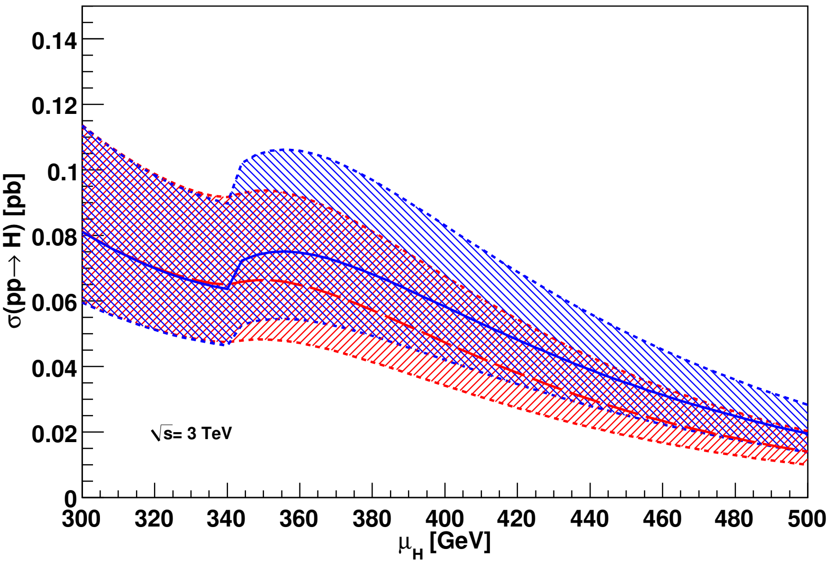

Figure 14: The production cross section $pp \to H$ at $\sqrt{s} = 3\,\mathrm{TeV}$ for CMRP (red, wide-dashed line) and CMCP (blue, solid line). The shaded areas surrounded by the dashed lines give the scale uncertainty obtained by varying $\mu_H/2 < \mu_R = \mu_F < 2\,\mu_H$ in the CMRP scheme and $\overline{\mu}_H/2 < \mu_R = \mu_F < 2\,\overline{\mu}_H$ (Eq.(18)) in the CMCP scheme. We have used MSTW2008 LO PDFs.

- $\mathbf{H \to \overline{b}b}$

Results for $H \to \overline{b}b$ are shown in Tab. 3 for the pure weak percentage one-loop corrections in the three schemes and for a wide range of Higgs masses; in Tab. 4 the electroweak (weak + QED) percentage one-loop corrections are given. For weak corrections the results for $H \to \overline{b}b$ are presented graphically in Fig. 18; the figure shows cusps at the $\overline{t}t$-threshold due to the fact that the top quark mass is kept real. The origin of the cusps is in a B_0-function with p^2 fixed at the complex Higgs pole. The size of the cusps can be related to the large Higgs width at the $\overline{t}t$-threshold as illustrated in Fig. 19 where we analyze $\mathrm{Re}\, B_0(-s_H\,;\, m_t, m_t)$ around the $\overline{t}t$ threshold. Here the solid line corresponds to $\gamma_H = 0$, whereas dash-lines correspond to increasing values of γ_H. As one can see the limit $\gamma_H \to 0$ is continuous and there is no artifact due to the analytical continuation. The wide-dashed blue line of Fig. 19 corresponds to a finite value of γ_H and to a complex top pole (with an on-shell width of 13.1 GeV).

As it is evident the introduction of a complex top quark pole completely cures the shape of the corrections. Therefore, this gives further evidence to using the CMCP scheme, at least from a theoretical point of view (the top quark total width is, unfortunately, poorly known). It is worth noting that the numerical effect given by the blue curve should be interpreted as an upper bound on the effect of a top quark complex pole since the experimental result is an upper bound, $\Gamma_t < 13.1\,\mathrm{GeV}$ at 95% C.L. Note that, from theory it follows $\Gamma_t^{\mathrm{LO}} = 1.47\,\mathrm{GeV}$ and $\Gamma_t^{\mathrm{NLO}} = 1.31\,\mathrm{GeV}$.

Finally, we observe that the $\mathcal{O}\left(\gamma_H/\mu_H\right)$ effects, which can reach several percent at large values of μ_H, have a modest effect on all those processes which start at $\mathcal{O}\left(g^2\right)$ (the effect being on NLO corrections) whereas the effect is considerably larger for those processes, e.g. $H \to \gamma\gamma(gg)$, which start directly at NLO ($\mathcal{O}\left(g^6\right)$).

10 Conclusions

In this paper we have shown how to continue Feynman integrals into the second Riemann sheet, in a way that can be easily implemented in any program aimed to compute pseudo-observables related to Higgs physics at Tevatron and LHC. Pseudo-observables give, in a natural way, the possibility of translating

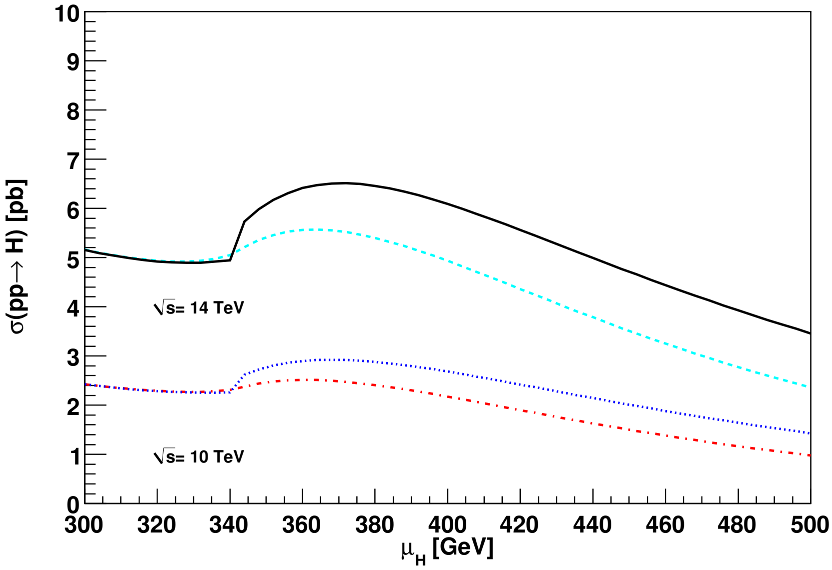

Figure 15: The production cross section $pp \to H$ at $\sqrt{s} = 10\,\mathrm{TeV}$ for CMRP (red, dashed-dotted line) and CMCP (blue, dotted line); at $\sqrt{s} = 14\,\mathrm{TeV}$ for CMRP (cyan, dashed line) and CMCP (black, solid line). We have used MSTW2008 LO PDFs with factorization scale $\mu_F = \mu_H$ for CMRP and $\mu_F = \overline{\mu}_H$ for CMCP.

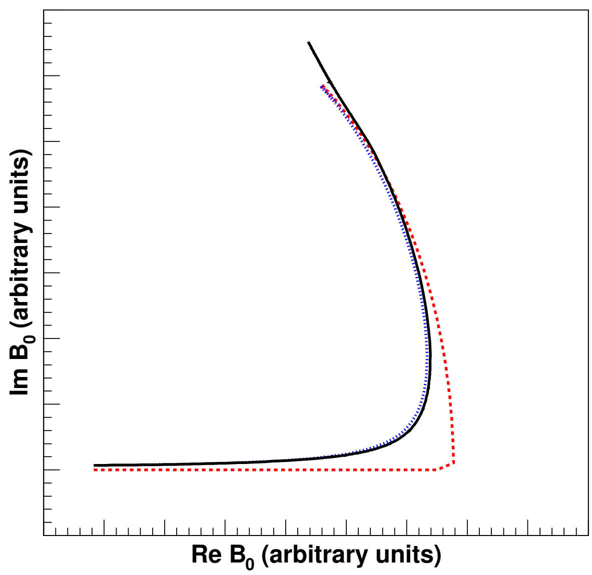

Figure 16: The scalar two-point function with two real internal masses (RMRP scheme) M_Z^2 or two complex internal masses (CMRP - CMCP schemes) s_Z. B_0 is computed in the RMRP (red dash-line), CMRP (blue dot-line) and CMCP (black solid-line) schemes. The Mandelstam invariant is μ_H^2 in the RMRP - CMRP schemes and s_H in the CMCP scheme, with $100\,\mathrm{GeV} < \mu_H < 500\,\mathrm{GeV}$. See Section 8 for the scheme definitions.

experimental data into a language that has a direct connection to unambiguous theoretical calculations. Using our framework one can freely compute quantities (otherwise non-existing) like Higgs production cross

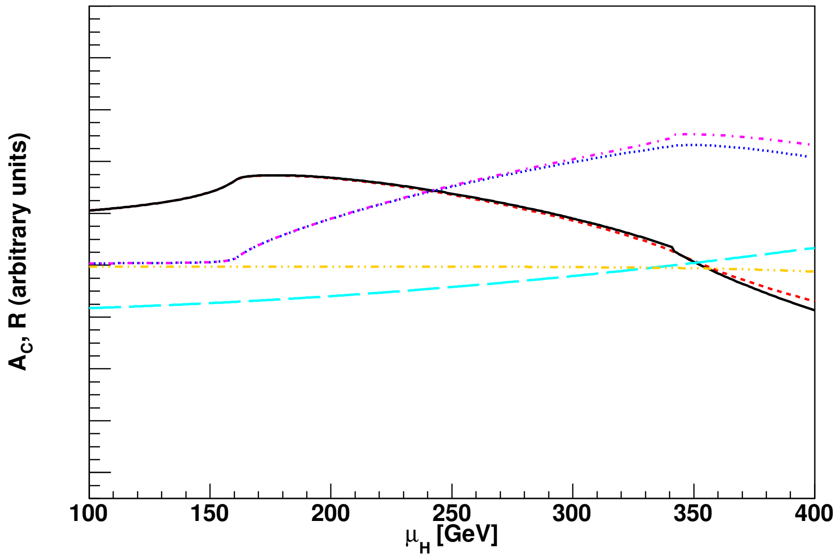

Figure 17: The C_0 part of the amplitude for $H \to \gamma\gamma$ and the corresponding rational term of Eq.(127) with $100\,\text{GeV} < \mu_H < 300\,\text{GeV}$. The black, solid (CMCP) and red, dashed (CMRP) lines give the real part whereas blue, dotted (CMRP) and magenta, dash-dotted (CMCP) lines give the imaginary part. The cyan, wide-dashed (orange, dash-double-dotted) line gives the rational real(imaginary) part of the amplitude without appreciable differences between the schemes. The imaginary part of the rational term is always small and negligible. See Section 8 for the scheme definitions.

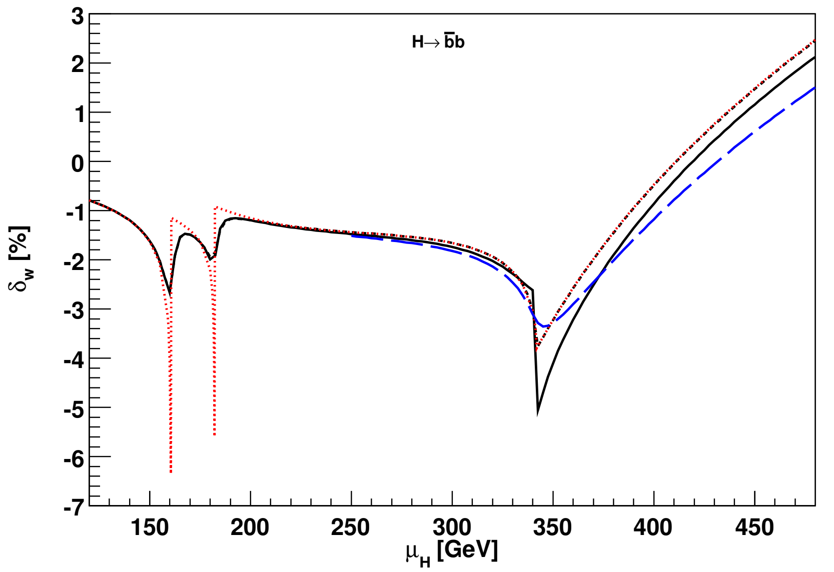

Figure 18: The weak one-loop radiative corrections to $H \to \overline{b}b$ in the RMRP scheme (red, dotted line), in the CMRP scheme (black, dashed line) and in the CMCP scheme (black, solid line). The effect of a complex top quark pole in CMCP (with a top total, on-shell, width of 13.1 GeV) is given by the blue wide-dashed line. See Section 8 for the scheme definitions. The result corresponding to $\Gamma_t = \Gamma_t^{\rm NLO} = 1.31\,\text{GeV}$ has no appreciable difference compared to the one at $\Gamma_t = 0$.

M_H [GeV]	δ_W RMRP [%] massless	δ_W CMRP [%] massless	δ_W CMCP [%] massless	δ_W CMCP [%] massive
120	-0.7890	-0.7904	-0.7904	-0.7837
130	-0.9557	-0.9572	-0.9573	-0.9509
140	-1.1978	-1.1986	-1.1986	-1.1922
150	-1.6215	-1.6146	-1.6149	-1.6078
160	-4.2656	-2.6458	-2.6690	-2.6587
170	-1.3987	-1.4914	-1.4875	-1.4822
180	-2.1989	-1.9435	-1.9912	-1.9858
190	-1.0338	-1.1744	-1.1590	-1.1569
200	-1.1547	-1.1967	-1.1987	-1.1974
210	-1.2452	-1.2621	-1.2730	-1.2723
220	-1.3132	-1.3198	-1.3379	-1.3376
230	-1.3647	-1.3665	-1.3914	-1.3917
240	-1.4047	-1.4044	-1.4363	-1.4370
250	-1.4376	-1.4365	-1.4759	-1.4769
260	-1.4674	-1.4665	-1.5138	-1.5151
270	-1.4985	-1.4981	-1.5539	-1.5555
280	-1.5357	-1.5361	-1.6008	-1.6026
290	-1.5851	-1.5865	-1.6604	-1.6624
300	-1.6557	-1.6582	-1.7410	-1.7431
400	-0.4736	-0.4865	-0.8589	-0.8633
450	$+1.4855$	$+1.4687$	$+1.1579$	$+1.1517$

Table 3: Percentage one-loop pure weak corrections for $H \to \overline{b}b$; the first entry is the RMRP scheme, the second entry is the CMRP scheme, the third entry is the CMCP scheme while the fourth entry is the CMCP scheme with finite m_b (Section 8).

section and Higgs partial decay widths.

An unstable particle cannot belong to the in/out basis of the Hilbert space, nevertheless concepts like production or decay of an unstable particle becomes aliases for pseudo-observables that have a well defined meaning and a direct relation to measured data.

In this paper a new scheme is introduced which is the (complete) complex mass scheme with complex, external Higgs boson (or, equivalently, any other external unstable particle) where the LSZ procedure is carried out at the Higgs complex pole (on the second Riemann sheet).

Pseudo-observables have been a very useful concept at LEP (e.g. Ref.[36]) and will continue to play an important role at LHC, although more difficult if deviations from the SM will emerge; in this case model independent approaches are required allowing for the extraction of useful quantities that can be fitted with different models.

The usual objection against moving standard model Higgs pseudo-observables into the second Riemann sheet of the S-matrix is that a light Higgs boson, say below 140 GeV, has a very narrow width and the effects induced are tiny. Admittedly, it is a well taken point for all practical consequences but one should remember that the Higgs boson width rapidly increases after the opening of the WW and ZZ channels and, because of this, the on-shell treatment of an external Higgs particle becomes inadequate as a description of data if the Higgs is not (very) light.

Furthermore, most of the experimental plots concerning Higgs physics extend well above, say, 200 GeV and, if a light Higgs boson is not discovered, one of the goals of LHC will be to exclude a standard model Higgs up to 600 GeV (see Ref. [37] for an exclusion plot of the SM Higgs boson for the various channels as well as the combination for masses up to 600 GeV). Already at 500 GeV the ratio CMCP/CMRP for the $gg \to H$ cross section is large and comparable to higher order QCD corrections.

M_H [GeV]	$\delta_{\rm EW}$ CMRP [%]	$\delta_{\rm EW}$ CMCP [%]
120	-0.9728	-0.9729
130	-1.1467	-1.1468
140	-1.3941	-1.3942
150	-1.8151	-1.8154
160	-2.8485	-2.8716
170	-1.7039	-1.7000
180	-2.1606	-2.2083
190	-1.3990	-1.3837
200	-1.4262	-1.4283
210	-1.4961	-1.5071
220	-1.5580	-1.5761
230	-1.6087	-1.6337
240	-1.6503	-1.6824
250	-1.6861	-1.7256
260	-1.7194	-1.7669
270	-1.7543	-1.8102
280	-1.7953	-1.8602
290	-1.8487	-1.9228
300	-1.9232	-2.0061
400	-0.7754	-1.1488
450	$+1.1697$	$+0.8571$

Table 4: Percentage one-loop electroweak (weak + QED) corrections for $H \to \overline{b}b$ with a massive b-quark; the first entry is the CMRP scheme, the second entry is the CMCP scheme (Section 8).

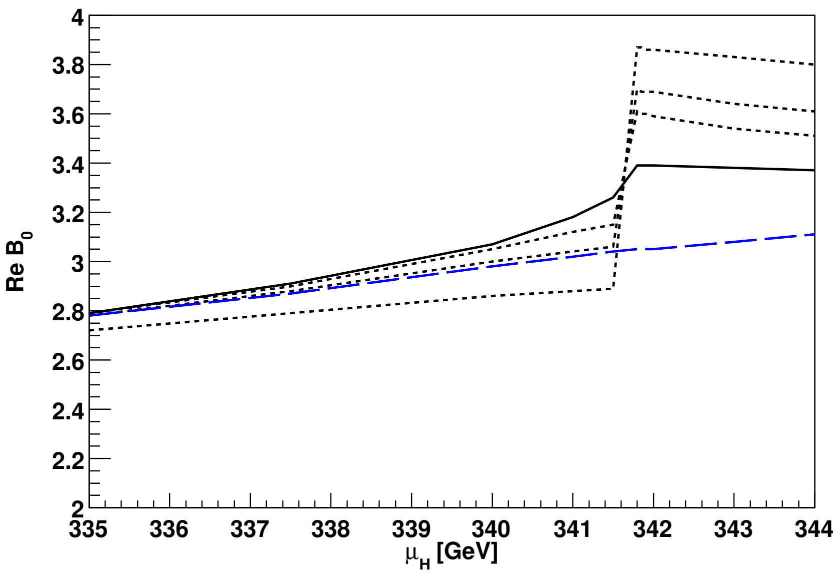

Figure 19: The $\mathrm{Re}\, B_0(-s_H\,;\, m_t, m_t)$ around the $\overline{t}t$ threshold. The solid line corresponds to a real Higgs mass, $\gamma_H = 0$, whereas dashed lines correspond to increasing values of γ_H. The blue, wide-dashed line corresponds to a finite γ_H and to a complex top quark pole (with an on-shell width of 13.1 GeV).

On top of all practical implications one should admit that it is hard to sustain a wrong theoretical description of experimental data if the correct one is available, independently on the size of the effect.

Finally, our results show that, above the $\overline{t}t$-threshold the Higgs-resonant contribution to $pp \to X$, correctly described in the CMCP scheme, is strongly influenced by the large imaginary part of the Higgs complex pole and the use of the conventional on-shell description of Higgs pseudo-observables becomes highly questionable, even from a numerical point of view.

Acknowledgments

G.P. is indebted to Stefan Dittmaier for an important discussion on $H \to 4\,$f. We gratefully acknowledge several discussions with W. Hollik and R. Pittau.

References

[1] T. N. Phenomena, H. w. group, f. t. C. collaboration and D. collaboration, arXiv:0903.4001 [hep-ex]; T. C. Collaboration, t. D. Collaboration, t. T. N. Physics and H. W. Group, arXiv:0911.3930 [hep-ex].

[2] J. Fernandez, f. t. ATLAS and C. Collaborations, arXiv:0905.1228 [hep-ex].

[3] C. Anastasiou, R. Boughezal and F. Petriello, JHEP **0904**, 003 (2009) [arXiv:0811.3458 [hep-ph]];
C. Anastasiou, AIP Conf. Proc. **806**, 75 (2006);
C. Anastasiou, K. Melnikov and F. Petriello, Phys. Rev. D **72**, 097302 (2005) [arXiv:hep-ph/0509014];
C. Anastasiou, K. Melnikov and F. Petriello, Phys. Rev. Lett. **93**, 262002 (2004) [arXiv:hep-ph/0409088];
C. Anastasiou and K. Melnikov, Nucl. Phys. B **646**, 220 (2002) [arXiv:hep-ph/0207004];
R. Boughezal, arXiv:0908.3969 [hep-ph].

[4] M. Grazzini, Nucl. Phys. Proc. Suppl. **183**, 25 (2008);
D. de Florian and M. Grazzini, arXiv:0901.2427 [hep-ph];
M. Grazzini, arXiv:0806.3336 [hep-ph].

[5] S. Actis, G. Passarino, C. Sturm and S. Uccirati, Phys. Lett. B **669** (2008) 62 [arXiv:0809.1302 [hep-ph]];
S. Actis, G. Passarino, C. Sturm and S. Uccirati, Nucl. Phys. B **811** (2009) 182 [arXiv:0809.3667 [hep-ph]];
G. Passarino, C. Sturm and S. Uccirati, Phys. Lett. B **655** (2007) 298 [arXiv:0707.1401 [hep-ph]].

[6] R. V. Harlander, H. Mantler, S. Marzani and K. J. Ozeren, arXiv:0912.2104 [hep-ph];
R. V. Harlander and K. J. Ozeren, JHEP **0911** (2009) 088 [arXiv:0909.3420 [hep-ph]];
R. V. Harlander and K. J. Ozeren, Phys. Lett. B **679** (2009) 467 [arXiv:0907.2997 [hep-ph]];
A. Pak, M. Rogal and M. Steinhauser, arXiv:0911.4662 [hep-ph];
A. Pak, M. Rogal and M. Steinhauser, Phys. Lett. B **679**, 473 (2009) [arXiv:0907.2998 [hep-ph]].

[7] R. E. Cutkosky, J. Math. Phys. **1** (1960) 429.

[8] M. J. G. Veltman, Physica **29**, 186 (1963).

[9] C. Mœller, K. Danske. Vid. Selsk. 22, no 19 (1946);
R. Peierls, Proceedings of the 1954 Glasgow Conference on Nuclear and Meson Physics, (Pergamon Press, New York, 1955) p. 296;
R. Jacob and R. G. Sachs, Phys. Rev. **121** (1961) 350.

[10] P. A. Grassi, B. A. Kniehl and A. Sirlin, Phys. Rev. Lett. **86** (2001) 389 [arXiv:hep-th/0005149];
B. A. Kniehl and A. Sirlin, Phys. Rev. Lett. **81** (1998) 1373 [arXiv:hep-ph/9805390];
B. A. Kniehl and A. Sirlin, Phys. Rev. D **77**, 116012 (2008) [arXiv:0801.0669 [hep-th]];
B. A. Kniehl and A. Sirlin, Phys. Lett. B **530**, 129 (2002) [arXiv:hep-ph/0110296].

[11] M. Beneke, A. P. Chapovsky, A. Signer and G. Zanderighi, Phys. Rev. Lett. **93** (2004) 011602 [arXiv:hep-ph/0312331].

[12] G. Valent, Nucl. Phys. B **65** (1973) 445;
J. Lukierski, Fortsch. Phys. **28** (1980) 259;
C. G. Bollini and L. E. Oxman, Int. J. Mod. Phys. A **8** (1993) 3185;
C. G. Bollini and L. E. Oxman, Int. J. Mod. Phys. A **7** (1992) 6845;

[13] R. S. Willey, Phys. Rev. D **59** (1999) 013009 [Erratum-ibid. D **61** (2000) 079902] [arXiv:hep-ph/9804392].

[14] D. Y. Bardin, M. Grunewald and G. Passarino, arXiv:hep-ph/9902452.

[15] R. G. Stuart, Phys. Lett. B **262** (1991) 113;
A. Sirlin, Phys. Rev. Lett. **67** (1991) 2127;
E. N. Argyres *et al.*, Phys. Lett. B **358**, 339 (1995) [arXiv:hep-ph/9507216];
W. Beenakker *et al.*, Nucl. Phys. B **500**, 255 (1997) [arXiv:hep-ph/9612260];
G. Passarino, Nucl. Phys. B **574** (2000) 451 [arXiv:hep-ph/9911482];
G. Passarino, Nucl. Phys. B **578** (2000) 3 [arXiv:hep-ph/0001212];
T. Bhattacharya and S. Willenbrock, Phys. Rev. D **47** (1993) 4022.

[16] P. A. Grassi, B. A. Kniehl and A. Sirlin, Phys. Rev. D **65**, 085001 (2002) [arXiv:hep-ph/0109228];
P. Gambino and P. A. Grassi, Phys. Rev. D **62**, 076002 (2000) [arXiv:hep-ph/9907254].

[17] S. Actis and G. Passarino, Nucl. Phys. B **777**, 100 (2007) [arXiv:hep-ph/0612124].

[18] A. Denner, S. Dittmaier, M. Roth and L. H. Wieders, Nucl. Phys. B **724** (2005) 247 [arXiv:hep-ph/0505042];
A. Denner and S. Dittmaier, Nucl. Phys. Proc. Suppl. **160** (2006) 22 [arXiv:hep-ph/0605312];
A. Denner, S. Dittmaier, M. Roth and D. Wackeroth, Nucl. Phys. B **560** (1999) 33 [arXiv:hep-ph/9904472].

[19] A. Ghinculov and T. Binoth, Phys. Lett. B **394** (1997) 139 [arXiv:hep-ph/9611357];
S. Willenbrock and G. Valencia, Phys. Lett. B **247** (1990) 341.

[20] T. Aaltonen *et al.* [CDF Collaboration], Phys. Rev. Lett. **102** (2009) 042001 [arXiv:0808.2167 [hep-ex]].

[21] H. A. Weldon, Phys. Rev. D **14** (1976) 2030.

[22] A. Bredenstein, A. Denner, S. Dittmaier and M. M. Weber, Phys. Rev. D **74** (2006) 013004 [arXiv:hep-ph/0604011];
A. Bredenstein, A. Denner, S. Dittmaier and M. M. Weber, JHEP **0702** (2007) 080 [arXiv:hep-ph/0611234];
C. Buttar *et al.*, arXiv:hep-ph/0604120.

[23] H. J. Bremermann and J. L. Durand J. Math. Phys. **2** (1960) 240.

[24] L. S. Brown, *Cambridge, UK: Univ. Pr. (1992) 542 p.*

[25] R. Erdelyi et al., *Higher Transcendental Functions vol. 1*, Bateman Manuscript Project (*McGraw-Hill 1953*).

[26] K. S. Kolbig, SIAM J. Math. Anal. **17** (1986) 1232. N. Nielsen, Nova Acta Leopoldina (Halle) **90** (1909) 123;
L. Lewin, Polylogarithms and associated functions, North Holland, Amsterdam, 1981.

[27] A. Ferroglia, M. Passera, G. Passarino and S. Uccirati, Nucl. Phys. B **650** (2003) 162 [arXiv:hep-ph/0209219].

[28] Z. Nagy and D. E. Soper, Phys. Rev. D **74** (2006) 093006 [arXiv:hep-ph/0610028].

[29] G. 't Hooft and M. J. G. Veltman, Nucl. Phys. B **153** (1979) 365.

[30] G. Passarino, Nucl. Phys. B **619** (2001) 257 [arXiv:hep-ph/0108252];
G. Passarino and S. Uccirati, Nucl. Phys. B **629** (2002) 97 [arXiv:hep-ph/0112004];
J. Bernstein, Modules over a ring of differential operators, Functional Analysis and its Applications 5(1971);
M. Sato, Nagoya Mat. J. **120** (1990) 1;
S. C. Coutinho, A Primer of Algebraic *D*-Modules, LMS Student Text 33 (1995);
F. V. Tkachov, Nucl. Instrum. Meth. A **389** (1997) 309 [hep-ph/9609429].

[31] S. Uccirati, Acta Phys. Polon. B **35** (2004) 2573 [arXiv:hep-ph/0410332].

[32] G. Passarino and S. Uccirati, Nucl. Phys. B **747** (2006) 113 [arXiv:hep-ph/0603121].

[33] V. S. Fadin, V. A. Khoze and A. D. Martin, Phys. Lett. B **320** (1994) 141 [arXiv:hep-ph/9309234].

[34] A. D. Martin, W. J. Stirling, R. S. Thorne and G. Watt, Eur. Phys. J. C **63** (2009) 189 [arXiv:0901.0002 [hep-ph]];
A. D. Martin, W. J. Stirling, R. S. Thorne and G. Watt, Eur. Phys. J. C **64** (2009) 653 [arXiv:0905.3531 [hep-ph]].

[35] D. de Florian and M. Grazzini, Phys. Lett. B **674** (2009) 291 [arXiv:0901.2427 [hep-ph]].

[36] M. W. Grunewald *et al.*, arXiv:hep-ph/0005309; D. Y. Bardin, M. Grunewald and G. Passarino, arXiv:hep-ph/9902452.

[37] ATLAS Collaboration, Expected Performance of the ATLAS Experiment, Detector, Trigger and Physics,CERN-OPEN-2008-020, Geneva, 2008;
G. L. Bayatian *et al.* [CMS Collaboration], J. Phys. G **34** (2007) 995.